Title

Deep scRNA sequencing reveals a broadly applicable Regeneration Classifier and implicates antioxidant response in corticospinal axon regeneration.

Journal

Neuron, 111(24)

Authors

Kim, Hugo

Saikia, Junmi

Monte, Katlyn

et al.

Publication Date

2023-12-20

DOI

10.1016/j.neuron.2023.09.019

Peer reviewed

HHS Public Access

Author manuscript

Neuron. Author manuscript; available in PMC 2024 December 20.

Published in final edited form as:

Neuron. 2023 December 20; 111(24): 3953–3969.e5. doi:10.1016/j.neuron.2023.09.019.

Deep scRNA sequencing reveals a broadly applicable Regeneration Classifier and implicates antioxidant response in corticospinal axon regeneration

Hugo J. Kim[1], **Junmi M. Saikia**[1,2], **Katlyn Marie A. Monte**[1], **Eunmi Ha**[1], **Daniel Romaus-Sanjurjo**[1], **Joshua J. Sanchez**[1], **Andrea X. Moore**[1], **Marc Hernaiz-Llorens**[1], **Carmine L. Chavez-Martinez**[1,3], **Chimuanya K. Agba**[1,2], **Haoyue Li**[1], **Joseph Zhang**[1], **Daniel T. Lusk**[1], **Kayla M. Cervantes**[1], **Binhai Zheng**[1,4,5,*]

[1]Department of Neurosciences, School of Medicine, University of California San Diego, La Jolla, California, USA

[2]Neurosciences Graduate Program, University of California San Diego, La Jolla, California, USA

[3]Graduate Program in Biological Sciences, University of California San Diego, La Jolla, California, USA

[4]VA San Diego Research Service, San Diego, California, USA

[5]Lead contact

Graphical Abstract

[*]Corresponding author: bizheng@health.ucsd.edu.

Author Contributions

Author 1: H.J.K. designed and executed the experiments, collected and analyzed data, and co-wrote the paper. Authors 2-14 contributed to various technical aspects and scientific discussion of the study. Corresponding Author 15: B.Z. conceived and supervised the work, co-wrote the manuscript.

Declaration of interests

The authors declare no competing interests.

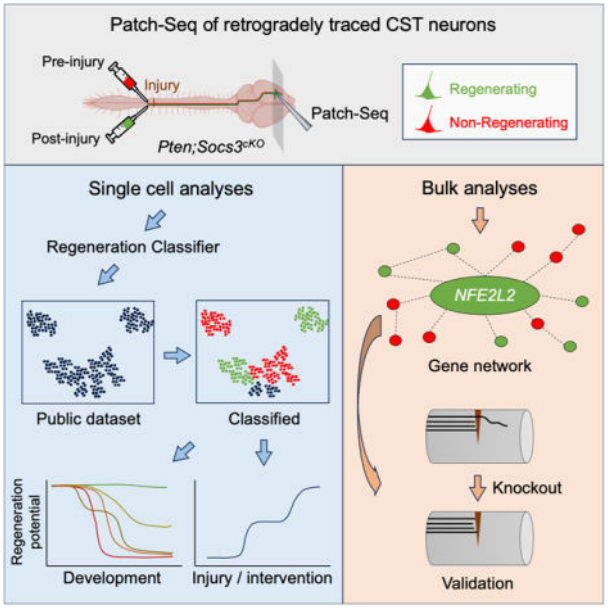

Through deep single cell RNA sequencing of regenerating corticospinal neurons, Kim et al. identify antioxidant response gene *NFE2L2* as a new regulator of axon regeneration and develop a Regeneration Classifier that can be broadly applied to predict the regenerative potential of diverse neuronal types based on their single cell transcriptomes.

SUMMARY

Despite substantial progress in understanding the biology of axon regeneration in the CNS, our ability to promote regeneration of the clinically important corticospinal tract (CST) after spinal cord injury remains limited. To understand regenerative heterogeneity, we conducted patch-based single cell RNA sequencing on rare regenerating CST neurons at high depth following *PTEN* and *SOCS3* deletion. Supervised classification with Garnett gave rise to a Regeneration Classifier, which can be broadly applied to predict the regenerative potential of diverse neuronal types across developmental stages or after injury. Network analyses highlighted the importance of antioxidant response and mitochondrial biogenesis. Conditional gene deletion validated a role for NFE2L2 (or NRF2), a master regulator of antioxidant response, in CST regeneration. Our data demonstrate a universal transcriptomic signature underlying the regenerative potential of vastly different neuronal populations, and illustrate that deep sequencing of only hundreds of phenotypically identified neurons has the power to advance regenerative biology.

INTRODUCTION

After spinal cord injury, axons from the corticospinal tract (CST) do not regenerate spontaneously to a significant extent. Extensive research has been conducted on the neuron intrinsic and extrinsic control of axon regeneration after CNS injury[1,2]. One of the first and more robust neuronintrinsic pathways manipulated to promote regeneration is the *PTEN/mTOR* pathway: genetic knockout or shRNA knockdown of *PTEN*, a negative regulator of *mTOR* signaling, promotes CST regeneration[3–5]. However, even with such

molecular interventions, only a few percent of CST axons regenerate, and this regeneration further declines with age[6]. Therefore, understanding the regenerative heterogeneity could be key to unlocking the mechanism of regeneration under a variety of pathophysiological conditions. In the retinal system, different retinal ganglion cell (RGC) subtypes are known to possess different regenerative capabilities and can differentially respond to molecular interventions[7,8]. Such regenerative heterogeneity has not been explored in the CST.

Single cell RNA sequencing (ScRNA-Seq) is a powerful tool to dissect the molecular heterogeneity among cells. Currently, most scRNA-Seq approaches involve tissue dissociation and random barcoding, sometimes aided by fluorescence-activated cell sorting (FACS) to purify the cells of interest[9]. Single cells in suspension are then sequenced using microfluidic devices such as the Chromium controller (10x Genomics)[10]. These methods are particularly suited to profile large numbers of cells in an unbiased manner, followed by bioinformatic analyses that define cell type taxotomy[11,12].

However, there are several drawbacks with these approaches when probing a very small, specific neuronal population with a particular phenotype, such as in the case of regenerating CST neurons. First, a very large number of cells need to be sequenced to reach a sufficient number of rare cells with the desired phenotype. With their somas residing in layer 5 of the sensorimotor cortex, CST neurons already represent a small portion of all cells through the cortical layers in the sensorimotor cortex. Assuming ~ 3% of CST neurons regenerating, we estimated that regenerating CST neurons in *PTEN*-deleted mice represent ~0.0118% of all cells in the cortical tissue harvested for scRNA-Seq [3% × 4K retrogradely labeled CST neurons / (6.8 mm^3 × 150K cells/mm^3)][13]. Thus, for every 100 regenerating CST neurons profiled, one would need to sequence ~0.85 million cells, the vast majority of which would not provide directly relevant information. Second, with a relatively low sequencing depth, the 10x Genomics-based methods may not detect subtle differences (e.g., on rare transcripts) among individual neurons of the same type. Third, cell dissociation and FACS may distort the transcriptome, especially for projection neurons with long processes[14].

These challenges can be addressed with a Patch-based scRNA-Seq method, which allows for high sequencing depth while its inherently low throughput does not present a barrier since our target neuronal population is very small. Patch-Seq was developed to capture the electrophysiological and morphological traits along with single cell transcriptomes on the same neurons, where the patch clamp pipette is repurposed to collect single cells from acute tissue slices[15,16]. Microscopy imaging can be integrated into the workflow to include morphological information, further expanding the multimodal capabilities of Patch-seq[17,18].

To this end, we have applied Patch-based scRNA-Seq to interrogate the transcriptomic profiles of regenerating vs non-regenerating CST neurons following *PTEN* and *SOCS3* deletion. Here we primarily used Patch-Seq as a method to collect neurons under visual guidance without employing its electrophysiological capabilities. To minimize PCR biases, we adopted a previously published linear amplification method that allows for high quality, deep sequencing of high complexity transcriptomes[19]. We show that deep sequencing even on as few as hundreds of CST neurons identified new candidates for regeneration regulators, and led to the development of a Regeneration Classifier that can be broadly applied to

predict the regenerative potential of diverse neuronal populations based on their single cell transcriptomes.

RESULTS

Experimental setup to differentially label regenerating CST neurons

We applied *PTEN* and *SOCS3* co-deletion to induce CST regeneration, as their co-deletion had previously been shown to synergistically promote axon growth (regeneration or sprouting) from RGCs and CST neurons[20,21]. To differentially label regenerating vs non-regenerating CST neurons, we applied two different retrograde viral tracers: one before and the other after a dorsal hemisection spinal cord injury (Figure 1A). Specifically, we applied the following surgeries on $PTEN^{fl/fl};SOCS3^{fl/fl};tdTomato^{fl/fl}$ mice along with $tdTomato^{fl/fl}$ control mice. First, we injected AAV-retro-Cre into the thoracic cord at low T8 level at 8 weeks of age to induce *PTEN* and *SOCS3* deletion and simultaneously activate the *Rosa26-lsl-tdTomato* reporter[22]. After 4 weeks, we applied dorsal hemisection injury 500 μm above the first injection site at T8. After another 6 weeks, we injected AAV-retro-GFP at low T8 (at the original AAV-retro-Cre injection level, 500 μm below injury). We expected that, in $PTEN^{fl/fl};SOCS3^{fl/fl};tdTomato^{fl/fl}$ mice, no more than a few percent of CST axons would regenerate ~500 μm beyond the injury site within the 10-week post-injury survival time and consequently pick up the 2nd tracer in green (GFP), whereas tdTomato would label both regenerating and non-regenerating neurons. Accordingly, green/red doubly (i.e., yellow) fluorescent CST neurons would have regenerated, while red (tdTomato) only CST neurons would most likely have not regenerated (Figure 1B,C).

Histological analyses on brain sections (Figure 1C, S1A) confirmed that GFP/tdTomato doubly fluorescent (regenerating) neurons represented only a small subpopulation of all CST neurons that were labeled in two $PTEN^{fl/fl};SOCS3^{fl/fl};tdTomato^{fl/fl}$ mice (559/15,451 = 3.6%); in contrast, no GFP labeled neurons were found in two $tdTomato^{fl/fl}$ control mice (0/22,849 = 0%), verifying no detectable CST regeneration without molecular intervention (Figures 1D; S1B,C). The apparent difference in the total number of retrogradely traced CST neurons between WT and $PTEN^{fl/fl};SOCS3^{fl/fl}$ mice (Figure S1B) was likely due to tracing variability and the low number (N = 2 / genotype) of mice assessed for histology only (Figure S1D). Despite tracing variability, it was clear that only *PTEN;SOCS3* deleted (but not WT) mice exhibited CST regeneration (Figure S1E).

Patch-based single cell sequencing

We used patch pipette to collect cytoplasmic material of 326 CST neurons (123 regenerating, 203 non-regenerating) from acute brain slices of 29 $PTEN^{fl/fl};SOCS3^{fl/fl};tdTomato^{fl/fl}$ mice. Cell collection was visually guided with both tdTomato and GFP fluorescent signals, although the setup we used did not allow for high resolution reconstruction of neuronal morphology (Figure 1E–J). These cells were processed using a modified aRNA linear amplification protocol[19], followed by standard Illumina TruSeq Stranded mRNA Library Prep. This method enabled us to conduct high quality, high depth sequencing of single cells. We targeted to sequence 5 million reads per cell, mapped uniquely to exons at ~1 million read pairs, which is ~100 times the depth of high quality

10x Genomics data (average 10K read pairs with sequencing saturation starting at 20K). The high sequencing depth allowed us to analyze the data using both single cell methods (Seurat, Garnett, SingleR) and bulk RNA-Seq methods (DESeq2, EdgeR). Because both regenerating and non-regenerating CST neurons underwent *PTEN;SOCS3* gene deletion, their transcriptomic differences do not necessarily reflect differences in PTEN/mTOR or SOCS3/STAT3 signaling. In the following, we describe our analyses with single cell methods first, followed by bulk-Seq analyses.

Seurat cluster analysis

For single cell methods, we analyzed the data using SingleR, Seurat, and Garnett. Following quality control (which removed 19 cells, resulting in 114 regenerating and 193 non-regenerating neurons), we applied SingleR[23] to transform our data into SingleCellExperiment objects, which classified the vast majority of the samples as neurons (304/307 = 99%) (Figure 2A). Only three cells exhibited astrocyte expression profile and were excluded from further analysis.

We conducted unsupervised clustering to determine whether regenerating and non-regenerating neurons would self-segregate based on their transcriptomes. UMAP-based Seurat analysis on all data yielded two strong clusters (number of marker genes=1780, FDR<0.05). (Figure 2B). DESeq2 analysis on Cluster 1 yielded 731 differentially expressed (DE) genes (661 overexpressed, 70 underexpressed) in regenerating neurons. While Cluster 1 is more balanced between regenerating and non-regenerating neuron, Cluster 2 is enriched in non-regenerating neurons (43 non-regenerating, 10 regenerating) (Figure 2C). There were no significant DE genes between regenerating and non-regenerating neurons within Cluster 2.

Building a Regeneration Classifier with Garnett

Unsupervised clustering above may not capture all transcriptomic features due to the relatively low sample size and the unusually high sequencing depth[24]. To gain further insights, we turned to an R package called Garnett, a supervised clustering tool to generate custom cell type classifier based on scRNA-Seq data[25]. Using both clusters found from Seurat and the regeneration phenotype within only Cluster 1 (i.e., without distinguishing the regeneration phenotype within Cluster 2), we trained the program to specifically detect regenerating CST neurons. Based on the p-value and logFC of markers found from DE genes in each cluster and between regenerating and non-regenerating neurons, we generated the marker file. With the marker file (initial marker genes listed in Figure 2D) and scRNA-Seq data, we trained the program to generate a Regeneration Classifier, which includes 4 groups: Regenerator, Non-regenerator, Unknown, and Cluster 2 (Figure 2C).

To start to assess the utility of the Regeneration Classifier, we applied it to a recent 10x v3 scRNA-Seq dataset on adult mouse primary motor cortex, which represents the cognate anatomical site for CST neurons[12]. Although a majority of glutamatergic neurons were classified as Non-regenerators, a substantial subset remained as Regenerators (Figure 2E,F). Subdividing glutamatergic neurons revealed cortical layer and neuronal projection-specific classifications (Figure 2G,H). Layer 5 (L5) extratelencephalically projecting neurons,

which include CST neurons, were among the least regenerating, with <20% classified as Regenerators (Figure 2I). (Note that regeneration ratio plots simply show the proportion of each group within the neuronal population: Regenerator, Non-regenerator, Unknown, and occasionally Cluster 2.) In comparison, a substantially higher proportion (~60–80%) of L6 intratelencephalically projecting neurons and L6b neurons were classified as Regenerators. L2/3 and L5 intratelencephalically projecting neurons fell in between. These observations are consistent with a previous *in vivo* imaging study indicating that L6 neurons exhibit a higher frequency of regeneration than L2/3/5 following laser axotomy[26]. Applying the Regeneration Classifier to scRNA-Seq data from adult raphe nuclei[27] classified most of the neurons (~96%) as Regenerators (Figure 2J), consistent with the observation in the literature that raphe nucleus-derived serotonergic (5-HT) axons regrow extensively after chemical or physical injury[28].

Regeneration classification reflects neurodevelopment stage across neuronal types—To systematically assess the validity of the Regeneration Classifier, we applied it to 21 published scRNA-Seq datasets on different neuron populations across developmental stages (Table S1; Figures 3, 4; S2–S4). There are two predictions for a valid Regeneration Classifier: 1) when applied to available scRNA-Seq data, it would delineate a general development-dependent decline in the regenerative potential of CNS neurons; 2) the exact temporal pattern of such a decline will vary depending on the specific neuronal type involved. Each dataset was analyzed for all cell types as well as for neurons only.

Applying the Regeneration Classifier to RGC data through different developmental stages (E13, E14, E16, P0, P5, P56)[29,30] indicates that: 1) most embryonic RGCs were classified as Regenerators, 2) most adult RGCs were classified as Non-regenerators, 3) there was a rapid conversion from Regenerators to Non-regenerators between P0 and P5, indicating a sharp decline in the regenerative potential (Figure 3A–G). Remarkably, this rapid drop in transcriptome-based regeneration potential closely mirrored the pattern of a precipitous decline in axon growth capacity at an early postnatal stage from previous *in vitro* studies[31] (Figure 3H).

We next extended this analysis to other regions of the nervous system from embryonic, postnatal, juvenile and adult stages, including forebrain/hindbrain, prefrontal cortex, sensory cortex, motor cortex, visual cortex, ventral midbrain, raphe nucleus, hypothalamus, cerebellum, spinal cord, and dorsal root ganglia (DRG)[12,27,32–48]. A detailed description of the specific datasets taken from each reference is listed in Table S1. Results indicate that, similar to RGCs, many neuronal types and CNS regions lose their regenerative potential between birth and postnatal day 23, roughly corresponding to the juvenile stage. This overall trend is best captured in Figure 4, where the percent of regeneration is calculated as the number of Regenerators over the sum of Regenerators and Non-regenerators (with the error bars representing extreme cases where Unknowns are either all Regenerators or all Non-regenerators).

Neurons in the ventral midbrain exhibit an earlier partial decline by around E15.5 (Figures 4; S2A–C). Sensory cortex, hypothalamus, prefrontal cortex, and visual cortex in turn lose their regenerative potential between P17–21 and P56 (Figures 4; S2D–H, S3). Note

that the precision of this timeline for any particular neuronal type was limited by the sampling frequency (e.g., postnatally for ventral midbrain, visual cortex). Motor cortex does not completely lose its regenerative potential by P56, reflecting some regenerative heterogeneity within cortical layers as discussed above (Figures 4, 2E–I). Likewise, spinal cord neurons exhibit an incomplete loss of their regenerative potential by P56, likely reflecting spontaneous regenerative ability of some spinal interneurons[49] (Figures 4; S4A–F). Cerebellum retains most of its regenerative potential by P17–21, the latest timepoint for which data were available (Figures 4; S4G–I). Raphe nuclei and DRG neurons retain most of their regenerative potential even by P56, a full adult stage (Figures 4, 2J; S4J–L, S7A,D).

Compared with adult CNS neurons, adult CNS non-neuronal cells tend to be classified more as Regenerators, sometimes displaying a salt-and-pepper pattern between Regenerators and Non-regenerators (e.g., Figures S2D, 3D,H). Together, these results illustrate that our Regeneration Classifier has strong predictive power for the regenerative potential across neuronal types, anatomical regions, and developmental timeline.

Applying Regeneration Classifier to other axon injury studies

Applying the Regeneration Classifier to scRNA-Seq data from published CNS injury studies revealed a partial transition from Non-regenerators to Regenerators that is accelerated by molecular interventions (Figures 5; S5, S6). Adult spinal neurons exhibit a notable baseline regenerative potential[36], again likely reflecting that of some interneurons (Figures 5A; S5A,B)[49]. Following spinal cord injury, a gradual transition occurred from Non-regenerators to Regenerators within the first 7 days post injury (Figure 5A). In the retinal system, adult RGCs exhibited a very low baseline regenerative potential, yet the same transition towards a high regenerative potential occurred within 7 days after optic nerve crush (Figure 5B; S5C–H)[30]. These data are consistent with a previous study indicating that neurons revert to a transcriptional growth state soon after injury without any molecular or cellular intervention[50]. With molecular interventions such as single, double or triple gene manipulations (involving *PTEN;SOCS3* loss of function and *CNTF* gain of function), this reversion is accelerated in RGCs, most notably with *PTEN*;*CNTF* double molecular intervention (Figures 5C; S6)[51]. While some of the unknown group may be due to insufficient transcriptomic information, the temporal pattern of transition after injury suggests that the unknown group may reflect a transitional state between Regenerators and Non-regenerators. In contrast, applying the Regeneration Classifier to DRG neuron data with multiple CNS and PNS injury models (including sciatic nerve injury, dorsal root crush, and spinal cord injury)[39,41] revealed a high pre-injury regenerative potential that sustained after injury (Figures 5D; S7).

Of all the published scRNA-Seq datasets we analyzed, Cluster 2 neurons were only identified in two studies, including one study involving *PTEN;SOCS3* deletion on RGCs[51], suggesting that Cluster 2 may bear features unique to *PTEN;SOCS3* gene deletion. We also developed a separate Regeneration Classifier by comparing regenerating and non-regenerating neurons from both clusters (instead of only Cluster 1). A limited analysis on two datasets[44,46] yielded similar results (data not shown), likely because the contribution from Cluster 2 was limited.

Limitations on applying Regeneration Classifier

Some variations exist between different published datasets (sometime even from the same research team), likely due to differences in the exact experimental paradigms / conditions, and the sequencing technologies used. Results from two DRG studies exhibited some discrepancies with other studies (Figures 5D; S4J–L, S7). Usoskin et al 2015 on adult DRGs[40] and Zeisel et al 2018 on juvenile DRGs[37] used the older technologies, while Avraham et al. 2020[39] used newer technologies, leading to some inconsistencies in the graph plotted for DRGs in Figure 4. Likewise, results from two injured RGC studies[30,51] also exhibited some differences, particularly notable at 7 days post injury without genetic manipulation (Figure 5B,C; S5G, S6C). Thus, intra-study comparisons are likely more accurate than inter-study comparisons.

Applying the Regeneration Classifier to published single nucleus RNA sequencing (snRNA-Seq) data of adult CNS neurons generated inconclusive data on three out of four datasets. Most neurons were unexpectedly classified as unknown in these three studies[52–54], which used the drop-seq (earlier version than Chromium 10x) or the 10x v2 kit (Figure S8A–C). The 4th study used the 10x v3 kit and generated distinct classifications, including retrogradely traced CST neurons that were classified mostly as Non-regenerators[55] (Figure S8D–F). Therefore, while the Regeneration Classifier is compatible with all scRNA-Seq datasets tested, it is less compatible with snRNA-Seq datasets likely due to the lack of cytoplasmic RNAs coupled with the older technologies that led to insufficient sequencing complexity[56].

Differential expression and gene network analyses

For bulk RNA-Seq methods, we analyzed differential gene expression with DESeq2 and EdgeR. DESeq2 gave 862 DE genes, with 711 overexpressed and 151 underexpressed genes in regenerating neurons as compared with non-regenerating neurons (FDR corrected p-value < 0.05, |log2 Fold change| > 1) (Figure 6A,B). Gene ontology (GO) analysis revealed that overexpressed genes (in regenerating neurons, as below) were enriched in ATP metabolic process (FDR = 7.51E-10), oxidative phosphorylation (FDR = 1.80E-08) and cellular respiration (FDR = 1.05E-7), indicating that mitochondrial activities are heavily involved in CST regeneration (Table S2).

Two top differentially overexpressed genes (based on log2 fold change, or logFC) include *ATP5A1* and *ATPIF1,* which are regulators of mitochondrial ATP synthesis, likely reflecting the requirement for high energy production during regeneration (Table S3A, Figure 6A). Other top differentially overexpressed genes include *SETD3*, *ATF4* and *EIF3F*. *SETD3* is an actin-specific histidine methyltransferase contributing to cytoskeleton integrity, and was recently found to mediate *PTEN* suppression-induced neuroprotection in an ischemia-reperfusion injury model by promoting actin polymerization and preserving mitochondrial function[57]. *ATF4* (Activating Transcription Factor 4) encodes a transcription factor of the cAMP response element-binding (CREB) protein family, which has another member, *ATF3*, extensively studied in peripheral axon regeneration. *EIF3F* (eukaryotic initiation factor 3F) is part of the *EIF3* complex that functions in the initiation of protein translation. Ingenuity Pathway Analysis (IPA) identified *EIF2* signaling as the top overexpressed canonical

pathway (Figure 6C), reaffirming the importance of protein synthesis. Other top pathways included oxidative phosphorylation, regulation of eIF4 and p70S6K signaling (related to mTOR and protein translation), Huntington's disease signaling, and mitochondrial dysfunction, among others.

Through gene network analyses on all DE genes (FDR<0.05, fold change>2), we found gene hubs that control large numbers of DE genes. Two hub genes that repetitively emerged from these analyses and regulate large numbers of DE genes were *NFE2L2* and *PPARGC1A* (Figure 6D,E). *NFE2L2* (nuclear factor erythroid-derived 2-like 2, also known as nuclear factor erythroid 2-related factor 2, or *NRF2*; not to be confused with another gene, nuclear respiratory factor 2, or *NRF-2*) encodes a transcription factor that activates antioxidant genes under oxidative stress in response to injury and inflammation[58,59]. *PPARGC1A* (peroxisome proliferator-activated receptor gamma coactivator 1-alpha, or PGC-1α) encodes a transcriptional co-activator that serves as a master regulator of mitochondrial biogenesis[60]. The Graphical Summary of IPA Core Analysis indicates that overexpression of *NFE2L2* (along with *PPARGC1B*, a homologue of *PPARGC1A*) is related to an increase in "Size of body" function, a decrease in cell death of tumor or cancer cells, and transport of molecules and vesicles (Figure 6F). Additional hub genes include regeneration promoters *MYC* and *IGF1R*. Direct upstream regulators included *RICTOR* (Inhibited, p=1.58E-33), *MLXIPL* (activated, 2.06E-24) and *MYC* (activated, p= 1.07E-21) (Table S4). RICTOR (Rapamycin-insensitive companion of mTOR) is a component of the mTORC2 complex, which has been shown to inhibit axon regeneration[61].

EdgeR, a weighted mean of log transformed method, detected 7751 DE genes (4813 overexpressed and 2948 underexpressed) in regenerating neurons (FDR p-value<0.05, |log2 fold change|>1) (Table S5A). GO analysis indicates that overexpressed genes are enriched in cytoplasmic translation, various metabolic processes, ATP biosynthetic process, and oxidative phosphorylation, among others (Table S5B), while underexpressed genes are enriched for localization functions such as cellular macromolecule localization and protein localization (Table S5D).

The top 20 differentially overexpressed genes (based on logFC) include *BCL11A* and *SNX4*. BCL11A (also known as CTIP1) interacts with calcium/calmodulin-dependent serine kinase (CASK) to regulate axon outgrowth and branching[62]. In yeast, the evolutionarily conserved *SNX4* fine-tunes the autophagic response via regulating intracellular trafficking following TORC1 inhibition[63]. Top 20 differentially underexpressed genes (based on logFC) in regenerating neurons include *KLF17* and *FOXG1* (Table S5C). KLF17 suppresses epithelial-mesenchymal transition and metastasis in a model of breast cancer[64], and members of the KLF family of transcriptional factors are known to regulate axonal growth and regeneration, with some promoting and others suppressing growth[65]. *FOXG1* encodes a transcriptional repressor highly expressed during neural development that functions in establishing neocortical organization and callosal projections[66].

Of the two different models (DESeq2 and EdgeR), there was an overlapping set of 609 DE genes (474 overexpressed, 135 underexpressed in regenerating neurons, representing ~67% and ~89% of DE genes detected with DESeq2). Overlapping genes proved to be strongly

significant in both EdgeR (FDR<0.01) and DESeq2 (FDR<0.001). The GO biological processes of overlapping overexpressed genes were enriched in oxidative phosphorylation and cellular respiration (Table S6A). GO biological process of overlapping underexpressed genes were enriched in neuron differentiation and macromolecule localization (Table S6B).

We compared our data with a published bulk RNA-Seq dataset on regenerating CST neurons following neural stem cell (NSC) transplant into a spinal cord injury site[50]. Despite the differences in the experimental paradigms including methods to induce CST regeneration, time after injury, and RNA-Seq techniques, we still found similarities between the two studies. From NSC transplant study, 2175 genes (38%) (E12 VS IP in three time points after injury) out of 5708 DE genes and 812 genes (36%) (Naïve VS IP in three time points after injury) out of 2228 were overlapped with our study based on EdgeR analysis. Among the 7751 DE genes in our data (FDR<0.05), the overlapping genes were 28% (E12 samples) and 10% (naïve samples). Similarly, 36% of the genes expressed differently in the injury only samples compared to the naïve sample overlapped with the published data (as shown in Table S7). These overlaps indicate that some regenerative pathways are shared even with vastly different regenerative interventions. Notably, our data also identified Huntington's Disease Signaling as a top canonical pathway (Figure 6C) and *Huntingtin* (*HTT*) as a top upstream regulator of DE genes (Table S4), as *HTT* was found to be a central hub in the NSC transplant study[50].

NFE2L2 deletion diminishes CST regeneration induced by PTEN deletion

Both *NFE2L2* and *PPARGC1A* emerged as central hubs of gene network and upstream regulators of DE genes in regenerating vs. non-regenerating CST neurons (Figure 6D,E). We thus pursued these as top candidates of new regeneration regulators, starting with *NFE2L2*. Because *NFE2L2* was hypothesized to positively regulate regeneration, we assessed the effect of *NFE2L2* deletion in *PTEN* deletion background, which provides an elevated level of baseline regeneration so that any reduction in regeneration could be detected.

We injected AAV-Cre to the sensorimotor cortex of $NFE2L2^{fl/fl}$;$PTEN^{fl/fl}$ mice along with $PTEN^{fl/fl}$ mice and wild-type (WT) control mice (Figure 7A). Four weeks later, mice were subjected to dorsal hemisection spinal cord injury. Six weeks later, BDA was injected into the sensorimotor cortex to anterogradely trace CST axons, and mice were sacrificed 2 weeks later. In injured mice of all three genotypes, transverse spinal cord sections 4–5 mm rostral to the T8 injury site exhibited anticipated CST axon patterns; 4–5 mm caudal to injury, no CST axons were detected, indicating lesion completeness (Figure S9A–F). There were no significant differences in the number of BDA-labeled CST axons in the medulla among the genotypes (Figures S9G–I, 7G).

As expected, WT mice exhibited no or little regeneration (Figure 7B), whereas *PTEN* deleted mice exhibited significant CST regeneration (Figure 7C)[3]. Strikingly, *PTEN* and *NFE2L2* co-deletion abrogated CST regeneration that is normally seen in *PTEN* deleted mice (Figure 7D). To quantify CST regeneration, axon densities at defined distances rostral to injury were normalized against the axon density at 1.5 mm rostral to injury; axon numbers at defined distances caudal to injury were normalized against total axon counts in the medulla, as described[67] (see Methods for details). This quantitative analysis verified

the qualitative observation: rostral to injury, *PTEN;NFE2L2* doubly deleted mice exhibited a modest decrease in CST axon density indices as compared to *PTEN* deleted mice, but did not reduce to WT levels; caudal to injury, double gene deletion abolished any CST regeneration induced by *PTEN* deletion (Figure 7E,F). Therefore, deleting *NFE2L2* reduces regeneration rostral to injury and regenerating axons especially have difficulty navigating beyond the injury site.

RNAscope in situ hybridization confirmed a substantial reduction of *NFE2L2* mRNA levels in mouse brains (Figure S10). As a control, we assessed CST axon pattern and total labeled axon counts in the medulla in a limited number of uninjured WT, *PTEN* and *PTEN;NFE2L2* conditional gene deletion mice, and found no overt differences among different genotypes (Figure S11). The number of mice examined for uninjured controls were low, at N = 2 per genotype; ideally, a minimum of N = 3 per genotype is desirable. Previous spinal cord regeneration studies examined N = 2–3 per genotype for uninjured controls of germline knockouts[68], or no uninjured controls for conditional knockouts[50] where there is less of a concern for developmental defects. The current study involves inducible, conditional knockout mice. This potential caveat is further mitigated by the normal looking CST axon patterns in injured *PTEN;NFE2L2* deletion mice in the medulla and the spinal cord rostral to the injury site (Figures S9, 7G). Together, these results identify NFE2L2 as a positive regulator of CST regeneration, and validate our Patch-Seq approach in discovering new regeneration regulators.

DISCUSSION

In this study, we adapted a Patch-seq workflow to conduct single cell sequencing on regenerating CST neurons following *PTEN;SOCS3* gene deletion. The unusually high sequencing depth afforded by this approach allowed us to conduct both single cell analyses such as Seurat and Garnett and bulk-Seq analyses on differential gene expression. The former led to the development of a Regeneration Classifier that exhibits predictive power for the regenerative abilities of a wide spectrum of neuronal types based on their single cell profiles. The latter led to the identification of new candidates of regeneration regulators, one of which, *NFE2L2* (also known as *NRF2*), has been validated by genetic analyses with an *in vivo* injury model. Thus, deep sequencing of even hundreds of neurons may reveal new biological insights into neuronal regeneration following spinal cord injury.

We used the Garnett R package to train a Regeneration Classifier based on DE genes within Cluster 1. We found that our Regeneration Classifier can be applied in an unbiased manner to characterize any published scRNA-Seq dataset. This generated a pattern of regeneration classification for various neuronal populations that remarkably reflects prior knowledge on their regenerative potential based on the neuronal type and developmental stage. Overall, embryonic neurons tend to be classified as Regenerators while adult neurons exhibit the opposite trend. Within adult neurons, while RGCs and many other CNS neuronal types exhibit a low regenerative potential, DRG and serotonergic neurons in the raphe nuclei exhibit a high regenerative potential based on the Regeneration Classifier, with other neuronal types falling in between. Applying the Regeneration Classifier to CNS injury datasets (CST neurons and RGCs) supports an emerging hypothesis that CNS neurons

revert to a regenerative state after injury[50], and further indicate that this reversion can be accelerated with molecular intervention. Because our Regenerative Classifier was developed based solely on data from CST neurons following *PTEN;SOCS3* deletion, these results indicate the existence of a broadly applicable transcriptomic signature underlying the regenerative abilities of diverse neuronal populations.

It has been extensively shown in the literature that neurons undergo a developmental stage-dependent decline in regenerative abilities. However, our data provide for the first time to our knowledge a transcriptomic basis for this phenomenon across vastly different neuronal types. Previous studies typically focused on one neuronal type at a time. Our study illustrates a broadly—potentially universally—applicable transcriptomic signature underlying the regenerative abilities of a diversity of neuron types as reflected by the Regeneration Classifier. Future studies will refine its predictive power. The Regeneration Classifier may be applied to pinpoint the critical transition time in development when neurons rapidly lose their regeneration abilities, as exemplified by RGCs (Figure 3G,H). The Regeneration Classifier may also be used to predict the regeneration-enhancing effects of various molecular and/or cellular interventions based on scRNA-Seq data given that these data are becoming widely available. This is especially useful when assessing many different experimental conditions such as combinatorial treatment or many different time points after injury and/or intervention. Because transcriptomic changes often precede phenotypic changes, prediction of regeneration based on scRNA-Seq data will provide a more sensitive way to capture a regenerative response than physiological readouts. For preclinical studies, a Regeneration Classifier may serve as a biomarker to predict the likelihood of success for candidate regenerative therapies. In this regard, our approach will likely have broad applicability in studying many other neurological conditions.

The Regeneration Classifier does not readily make predictions on whether a more regenerative neuronal type will be more amenable to regeneration-promoting manipulations, especially one targeting *PTEN;SOCS3*. For instance, 5-HT neurons in the raphe nuclei exhibit robust spontaneous regeneration[28] and are classified as such in the current study (Figures 2J, 4). Previous work indicates that targeting PTEN pharmacologically enhances 5-HT axon growth after spinal cord injury[69]. However, genetically targeting *PTEN;SOCS3* has not been tested on 5-HT axon regeneration. While this would be an interesting experiment to pursue in its own right, either positive or negative outcome will not validate or invalidate the Regeneration Classifier. Manipulations developed for the regeneration-resistant CST neurons may or may not work well on the robustly regenerating 5-HT neurons. In our Patch-seq experiments, both regenerating and non-regenerating neurons underwent *PTEN;SOCS3* deletion. Thus, the difference in their regenerative abilities may not rely on their *PTEN;SOCS3* status. The observation that the Regeneration Classifier can be broadly applied to many neuronal types covering 22 published scRNA-Seq studies (Table S1, Figures 3–5, S2–S7) strongly suggest that the different regenerative abilities detected by Regeneration Classifier are not dependent on *PTEN;SOSC3*. Future studies are required to untangle the complexity involving scRNA-Seq data based regeneration prediction and neuron type-specific molecular interventions to promote regeneration.

There are instances where the Regeneration Classifier appears to break down either biologically or technically. Biologically, it is well known that DRG neurons exhibit different regenerative outcomes (i.e., robust regeneration after PNS injury, but only limited regeneration after CNS injury); however, our Regeneration Classifier uniformly predicted DRG neurons to be robustly regenerating regardless of CNS or PNS injuries (Figure 5D). This could mean that the Regeneration Classifier, developed on a regeneration-resistant CNS neuronal type, works well for CNS but not PNS neurons. Meanwhile, it could also mean that the Classifier only captures neuron-intrinsic ability to regenerate, while neuron-extrinsic factors additionally influence the regenerative outcome. In reality, this is likely more complex, as DRG neurons have been shown to elicit different transcriptional programs after CNS vs PNS injuries. Technically, three out of four snRNA-Seq datasets analyzed did not generate useful predictions (Figure S8A–C), likely due to the low transcriptomic complexity resulting from the lack of cytoplasmic RNAs in conjunction with the older generation 10x Genomics platforms. One snRNA-Seq study with the newer 10x Genomics v3 platform (Beine et al., 2022) generated useful predictions (Figure S8D–F). As more labs adopt the newer 10x Genomics platforms with higher transcriptomic complexities, the current Regeneration Classifier will likely be sufficient to make useful predictions on new snRNA-Seq data. Its predictive power may be further improved by sequencing more CST neurons, CST neurons with different regenerative interventions, or other neuronal types following molecular intervention.

The GO and IPA analyses illustrated the importance of protein translation, oxidative stress response, and mitochondrial biogenesis/function in CST regeneration. Regenerating CST neurons differentially overexpress genes and pathways involved in protein translation including *eIF2*, *eIF3F*, *eIF4* and *p70S6K*. This is in line with the published literature on *PTEN/mTOR* and other pathways demonstrating the importance of protein synthesis in CNS axon regeneration[3,70]. Other genes/pathways known to regulate axon growth and regeneration were also captured in our study, such as *MYC*, *IGF1R* and *HTT* (Table S4). MYC overexpression synergizes with *PTEN;SOCS3;CNTF* manipulations to promote robust retinal axon regeneration after optic nerve crush[71]. Administration of IGF1R antibodies blocks CST axon extension in the postnatal spinal cord[72]. HTT (Huntingtin) mediates host CST axon regeneration into neural stem cell graft implanted at a spinal cord injury site[50].

Compared with protein translation, much less is known about the role of antioxidant response and mitochondrial biogenesis in CNS axon regeneration. In our study, *NFE2L2* and *PPARGC1* emerged as two top upstream regulators of pathways enriched in regenerating neurons. It should be noted that signaling pathways involving *NFE2L2* and *PPARGC1* — and not necessarily their own expression levels—were predicted be upregulated in regenerating neurons. *NFE2L2* (*NRF2*) encodes a master regulator of the antioxidant defense system[73]. Upon oxidative stress, NRF2 enters the nucleus and mediates the transcription of antioxidant genes through binding to an enhancer element called antioxidant response element (ARE). Extensive studies have shown a cytoprotective role for NRF2 in a variety of pathological conditions including inflammation, cancer, cardiovascular and neurodegenerative diseases. *NFE2L2;PTEN* double gene deletion abolishes CST regeneration induced by *PTEN* deletion, pointing to an important role for NRF2-mediated antioxidant response in CST regeneration. As aging reduces the expression level of NRF2[74],

this may partially account for the age-dependent decline in CST regeneration previously reported with PTEN deletion[6]. Conversely, a previous study indicates that reactive oxygen species (ROS) is required for peripheral and dorsal column sensory axon regeneration[75]. Thus, the complex roles of ROS, oxidative stress and antioxidant defense system, including any neuronal type-specific regulation, remain to be fully elucidated.

Another top candidate, *PPARGC1A* (or *PGC-1α*), encodes a master regulator of mitochondrial biogenesis[76]. The role of PGC-1α in CST regeneration awaits to be validated *in vivo* with function perturbation experiments. Nevertheless, our observation that these two genes (*NFE2L2, PPARGC1A*) sit at the top of the regulatory network in regenerating neurons highlights the importance of both antioxidative response and mitochondrial biogenesis. Indeed, mitochondrial function and dysfunction are intimately linked to oxidative stress and redox state within the cells. There is evidence that *NFE2L2* cross-regulates with genes involved in mitochondrial biogenesis and function[77]. Conversely, PGC-1α has a role in antioxidant response[78], and can co-activate the transcription of *NFE2L2*[59]; PGC-1α and NFE2L2 may even cross regulate[79]. Thus, resolving oxidative stress and maintaining healthy mitochondria function are likely two important and related aspects of CST axon regeneration. Previous studies stressed a role for mitochondrial motility and energy metabolism in CNS regeneration[80–82]. The current study emphasizes the importance of countering the negative consequences of mitochondrial dysfunction. While our initial *in vivo* validation focused on loss of function analyses as they tend to better reflect the physiological functions of endogenous genes, future studies are required to ascertain whether overexpressing NFE2L2 (or PGC-1α) will promote regeneration. Other top candidates of positive regulators such as SETD3 may lead to additional biology insights. In addition, candidate negative regulators of regeneration can be suppressed to enhance regeneration.

Our work highlights the value of deep sequencing on a relatively small number of neurons in studying the biology of CNS axon regeneration. As such, deep sequencing of even hundreds of CST neurons may lead to the identification of new regeneration regulators and the development of a widely applicable Regeneration Classifier, which has likely benefited from the Patch-Seq work flow and a linear amplification method resulting in an unusually high sequencing complexity[19]. A recent study applying high depth SMART-Seq2 to hundreds of FACS-purified RGCs demonstrated that high depth, low sample size sequencing can distinguish two rare, transcriptionally similar neuronal subtypes that could not be distinguished with droplet-based scRNA-Seq[83]. Therefore, high depth, low throughput scRNA-Seq methods have a unique niche in distinguishing transcriptionally similar neuronal subtypes or even states. In our study, the differential gene expression between regenerating and non-regenerating CST neurons reflected the different regenerative states rather than neuronal subtypes. High depth, low throughput scRNA-Seq methods will continue to complement low depth, high throughput methods in understanding new biology.

STAR METHODS

Lead contact

Further information and requests for resources and reagents should be directed to and will be fulfilled by the lead contact, Binhai Zheng (bizheng@health.ucsd.edu).

Materials availability

Request for resources and reagents should be directed to the lead contact. This study did not generate new unique reagents.

Data and code availability

- Single-cell RNA-seq data have been deposited at GEO and are publicly available as of the date of publication. Accession numbers are listed in the key resources table. Raw histological data were deposited on Mendeley at: https://data.mendeley.com/v1/datasets/10.17632/fywzyvgnkb.1
- All original code has been deposited at GitHub and is publicly available as of the date of publication. DOIs are listed in the key resources table.
- Any additional information required to reanalyze the data reported in this paper is available from the lead contact upon request.

Experimental model and study participant details

Mice—We used *PTEN*$^{fl/fl}$;*SOCS3*$^{fl/fl}$;*tdTomato*$^{fl/fl}$ mice for Patch-Seq experiments and *tdTomtato*$^{fl/fl}$ mice for control. Cre mediated recombination induces gene deletion for *PTEN* and *SOCS3*, and simultaneously activates the *tdTomato* reporter gene targeted to the ROSA26 locus. *PTEN*$^{f/f}$; *SOCS3*$^{f/f}$;*tdTomato*$^{f/f}$ line was inherited from previously published studies[85]. The age of mice used were 8 weeks after birth. For *NFE2L2* function validation experiment using genetic loss of function, we used *NFE2L2*$^{fl/fl}$ mice from Jackson Laboratory (C57BL6-*Nfe2l2*$^{tm1.1Sred}$/SbisJ ,Strain #: 025433) and bred this line to *PTEN*$^{fl/fl}$ mice to obtain *NFE2L2*$^{fl/fl}$;*PTEN*$^{fl/fl}$ mice. The age of mice used were 6 weeks after birth. In all experiments, both males and females were used in approximately 1:1 ratio, and we did not observe any overt sexual dimorphism in this study. All mice were assessed in C57BL/6 background. All procedures were approved by the Institutional Animals Care and Use Committee at University of California San Diego and at VA San Diego.

Method details

Mouse surgeries—We performed three mouse surgeries prior to Patch-Seq based cell collection. At the age of 8 weeks, AAV-retro-Cre (10^13 gc/ml titer, Boston Children's Hospital Viral core; same below) was injected to low T8 level of the spinal cord. Using a 10 μl Hamilton Syringe with a glass pipette attachment, we injected 0.8 μl virus at 0.1 μl/min to 0.5 mm left from the center of the spinal cord and 0.5 mm deep unilaterally. Four weeks after the first injection, dorsal hemisection (0.7 mm depth) was performed 0.5 mm above the injection site at T8, as previously described to lesion the main and dorsolateral CST axons[6,67]. A pair of superfine straight vannas scissors (Cat # 501778, WPI) were

used to cut the dorsal half of the spinal cord in multiple cuts at 0.7 mm depth, and the injury completeness was ensuring by passing a microfeather blade at 0.7 mm depth (Cat # 200300715, pfm medical) once in both directions. After 6 weeks, AAV-retro-GFP (10^13 gc/ml titer) was injected at the same injection site for the first injection. Four weeks after the second injection, we sacrificed the mice and collected single cells using a patch clamp setup. The contralateral hemispheres were kept in 4% Paraformaldehyde (PFA). In addition, a small number of mice (2 *tdTomato*$^{fl/fl}$ control and 2 *PTEN*$^{fl/fl}$*;SOCS3*$^{fl/fl}$*;tdTomato*$^{fl/fl}$ mice) underwent the same procedures but were perfused with 4% PFA and used solely for immunohistochemical examination and quantification of retrogradely labeled CST neurons.

For *NFE2L2* function validation experiment, we performed three mouse surgeries prior to the terminal procedures. At the age of 8 weeks, we injected AAV-Cre (10^13 gc/ml titer) Virus at a rate of 0.1 μl/min for 4 min, total 0.4 μl per injection unilaterally at 0.5mm depth to the hindlimb-projecting sensorimotor cortex after craniotomy (Coordinate: 1.4 mm lateral, 0.1 mm posterior; 1.0 mm lateral, 0.6 mm posterior; and 1.4 mm lateral, 1.1 mm posterior from bregma) as previously described[6,67] After 4 weeks, we perform the dorsal hemisection spinal cord injury at T8. After 6 weeks, biotinylated dextran amine (BDA, Cat # D1956, Invitrogen) was injected into the same coordinates of the cortex as AAV-Cre above to trace CST axons. Mice were sacrificed 2 weeks after the BDA injection with pentobarbital followed by PFA perfusion. For uninjured mice, we injected AAV-Cre into the cortex at the same coordinates, waited 3 weeks and performed PFA perfusion.

Immunostaining and microscopy imaging—For quantification of retrogradely labeled CST neurons, the perfused brain blocks from 2 *tdTomato*$^{fl/fl}$ (control) and 2 *PTEN*$^{fl/fl}$*;SOCS3*$^{fl/fl}$*;tdTomato*$^{fl/fl}$ mice were cut in 20 μm coronal sections from rostral to caudal in 1X PBS, and DAPI (1:5000) was applied to stain the nuclei and sections were mounted on Superfrost Plus slides and Fluoromount-G was used as the mounting medium. The slides were visualized under a Zeiss AxioImager M1 fluorescence microscope using separate filters for GFP, tdTomato and DAPI. GFP and tdTomato were visualized with their native signals without immunostaining. Images were taken and the numbers of neurons carrying GFP and/or tdTomato signals were quantified. Three additional contralateral hemispheres from *PTEN*$^{fl/fl}$*;SOCS3*$^{fl/fl}$*;tdTomato*$^{fl/fl}$ mice (with the ipsilateral side previously used for Patch-Seq collection) were processed in the same way for quantification.

For *NFE2L2* function validation experiment, sagittal spinal cord and transverse medulla sections were stained with rat anti-GFAP primary antibody (Cat # 13–0300, ThermoFisher) and anti-Rat secondary antibody conjugated with Alexa 488 (Cat # A-11006, ThermoFisher). BDA was stained with ABC kit (PK-4000 , Vector Labs) and TSA reagent Cy3.5 (NEL744001KT, Perkin Elmer), as described[67]. Tissue sections were imaged with 10x and 20x objectives. To assess CST regeneration, we quantified the rostral axon density indices and the caudal axon number indices as previously described[67,85]. Specifically, labeled CST axon densities measured at defined distances rostral to the injury site were averaged over ~10 sagittal sections and then normalized against the axon density at 1.5 mm rostral to injury; labeled CST axon numbers counted at defined distances caudal to the injury site were averaged over ~10 sagittal sections and then normalized against total axon

counts in the medulla. All quantifications were conducted by experimenters blinded to the genotypes, sometimes by multiple experimenters independently to check the results. The same procedure on medulla counts was performed for the uninjured mice.

RNAscope—To confirm conditional *NFE2L2* gene deletion in brain tissue, a custom fluorescent RNAscope Multiplex Fluorescent V2 Assay (ACD Biotechne, Cat #323100) was used to detect mRNA. Probes targeting *NFE2L2* (exon 5) and *Bcl11b* (marker for CST neurons) were used. For each experimental or control condition, coronal brain sections measuring 20 μm in thickness from three mice per genotype were selected spanning the region of AAV-Cre injections. The sections were mounted and baked onto Superfrost Plus slides (Thermo Fisher Scientific) and blocked for endogenous peroxidase activity; subsequently slides underwent antigen retrieval treatment and allowed to dry overnight. On the following day, sections underwent protease treatment, and probes were hybridized and amplified. Signal was detected with TSA Vivid™ Fluorophore Kit 570 (Tocris, Cat #7526) and TSA Vivid™ Fluorophore Kit 520 (Tocris, Cat #7523), and counterstained with DAPI for nuclei; 10× images were taken spanning the entire cerebral cortex, and 20× images were taken at Layer 5.

Patch clamping and single cell extraction—Mice were sacrificed with Ketamine/Xylazine mix followed by perfusion with bubbling sucrose cutting solution and decapitation. Mouse brains were sliced with VT1000 vibratome (Leica) into 200–400 μm slices. Neurons in acute brain slices were visually identified under illumination with an infrared Dodt Gradient Contrast system (Scientifica) and fluorescence (488 and 594 nm). Patch pipettes (6–10 MOhm; 1.2 mm O.D.) were filled with intracellular solution (K-gluconate 130 mM; KCl 2 mM; $CaCl_2$ 1 mM; MgATP 4 mM; GTP 0.3 mM; phosphocreatine 8 mM; HEPES 10 mM; EGTA 11 mM; pH 7.25 and 300 mOsm) containing 0.4 U/μl recombinant RNase inhibitor (Clontech).

Under the Dot contrast, the suction pipette was used to remove the top layer of the tissue slice including dead debris and connective tissue to expose CST neurons. Then, the patch pipette tip was lowered. Using red fluorescence (tdTomato), CST neurons were identified, and patch pipette was approached to the cell to form a giga seal. After making whole cell configuration, using the strong attachment, the entire cell on patch pipet was lifted straight out of the solution. The content was expelled into a PCR tube containing 5 μl of lysis buffer (made using NaCl 350 mg, Triton 500 μl, NP-40 500 μl, deoxy 2.5 ml, Tris HCl pH 8.8 1 ml, Tris HCl pH 6.8 1.5 ml, HEPES 240 mg, pH adjusted to 8) by breaking the end of pipette tip and immediately flash frozen using liquid nitrogen. The cellular material was centrifuged followed by 1 to 2 freeze thaw cycles to ensure complete lysis of the material.

Modified aRNA protocol—We processed collected single cells using the modified aRNA protocol previously described[19] followed by Illumina TruSeq Stranded mRNA library prep (Cat # 20020594, Illumina).

Sequencing and data processing—Size distribution of sequencing libraries was assessed by Agilent D1000 Screen Tape (5067–5582) on an Agilent 2200 TapeStation, and library concentrations were measured by Qubit from the IGM Genomics Center at UC San

Diego. Libraries were multiplexed and sequenced on an Illumina NovaSeq System with 150 bp pair-ended reads and trimmed to 100 bp reads.

Sequencing reads were further trimmed from both ends based on quality score. The trimmed reads were mapped to mouse genome (Release M22, GENCODE) using STAR aligner (STAR - 2.5.3a) at the Triton Shared Computing Cluster (TSCC), UC San Diego[95]. Mapped samples were processed using HTSeq and made into read tables.

Data analysis and developing Regeneration Classifier—Because our Patch-Seq data with linear amplification is different from regular 10x based single call data or bulk RNA, we used both DESeq2 and EdgeR to identify differentially expressed (DE) genes. We conducted Gene Ontology (GO) analysis using the gene list and p-values from our data using topGO package. For clustering, we generated a Seurat object from the data and ran through the Seurat workflow. Cell types were initially classified using SingleR package. Upon publication, we will share our code in the following GitHub page: https://github.com/neurohugo/SingleCellPatchseqAnalysis.

We generated the Regeneration Classifier from the DE genes in regenerating neurons of Cluster 1 using Garnett[25]. We used Garnett to train cell type classifier using the dataset we obtained in this study, and applied it to other datasets from the scRNAseq package (Bioconductor)[96] and published papers (listed in Supplemental Table 1). All data were transformed into Seurat objects[97] and classified using the Regeneration Classifier. Using the Regeneration Classifier, we also generated the package “RegenOrNoRegen”, which is available in the same GitHub page.

The Ingenuity Pathway Analysis (IPA) was done with two different methods. First, for the independent network analysis, we applied all DE genes to the field and connected them together. Then we applied the Grow function to expand the network, limited only one step upstream. We removed all the unconnected genes and organized hierarchically to find the hub genes. In addition, we independently applied the Core Analysis and Graphical Summary.

Quantification and Statistical Analysis—We assumed that all the data are following normal distribution. For the brain counts, we performed the standard one-tailed *t*-test between two groups ($PTEN^{fl/fl};SOCS3^{fl/fl};tdTomato^{fl/fl}$ mice along with $tdTomato^{fl/fl}$ controls) using GraphPad Prism 9.0 software. The GraphPad Prism software doesn’t allow us to perform *t*-test when all the values are the same (at zero), so we added 0.000001 to one of the samples. We separately applied *t*-test using Excel and obtained the same *p*-value (Figure 1).

For differential expression analysis, we used DESeq2 and EdgeR packages in R software. We used the FDR adjusted *p*-value calculated by the program and set 0.05 as the threshold for statistical significance (Figure 6, Supplementary Tables S2–S7). The network core analysis was performed using Ingenuity Pathway Analysis (IPA) with the adjusted *p*-values calculated by the software.

For the *PTEN;NFE2L2*^{cKO} regeneration cohort, we applied two-way RM ANOVA with GraphPad Prism in both rostral and caudal quantifications (Figure 7), as described previously[67]. Detailed description is provided in figure legend.

Supplementary Material

Refer to Web version on PubMed Central for supplementary material.

Acknowledgement

We thank Dr. Matthew Banghart, Dr. Kim Dore, Dr. Mark Tuszynski and Dr. Roberto Malinow for generously allowing us to use their patch clamp rigs for the patch-seq studies described here. We thank Geneva Le, Andrea Luna and Kristen Tsai for technical assistance. This work was funded by grants from NIH (NS093055), VA (RX002483), and Craig H. Neilsen Foundation (733544) to B.Z. H.J.K. was supported by a Craig H. Neilsen Foundation Postdoctoral Fellowship (648861). C.L.C and C.A were supported by NIH genetics training grants (GM008666, GM145427). All sequencing was conducted with an Illumina NovaSeq 6000 at the UC San Diego IGM Genomics Center (supported by NIH S10 OD026929) or Novogene. Viral preps were obtained from Boston Children's Hospital Viral Core (EY012196). The contents do not represent the views of the US Department of Veterans Affairs or the United States Government.

Inclusion and diversity

We support inclusive, diverse, and equitable conduct of research.

REFERENCES

1. Sofroniew MV (2018). Dissecting spinal cord regeneration. Nature 557, 343–350. 10.1038/s41586-018-0068-4. [PubMed: 29769671]
2. Zheng B, and Tuszynski MH (2023). Regulation of axonal regeneration after mammalian spinal cord injury. Nat. Rev. Mol. Cell Biol, 1–18. 10.1038/s41580-022-00562-y. [PubMed: 36319695]
3. Liu K, Lu Y, Lee JK, Samara R, Willenberg R, Sears-Kraxberger I, Tedeschi A, Park KK, Jin D, Cai B, et al. (2010). PTEN deletion enhances the regenerative ability of adult corticospinal neurons. Nat. Neurosci 13, 1075–1081. 10.1038/nn.2603. [PubMed: 20694004]
4. Lewandowski G, and Steward O (2014). AAVshRNA-Mediated Suppression of PTEN in Adult Rats in Combination with Salmon Fibrin Administration Enables Regenerative Growth of Corticospinal Axons and Enhances Recovery of Voluntary Motor Function after Cervical Spinal Cord Injury. J. Neurosci 34, 9951–9962. 10.1523/JNEUROSCI.1996-14.2014. [PubMed: 25057197]
5. Zukor K, Belin S, Wang C, Keelan N, Wang X, and He Z (2013). Short Hairpin RNA against PTEN Enhances Regenerative Growth of Corticospinal Tract Axons after Spinal Cord Injury. J. Neurosci 33, 15350–15361. 10.1523/JNEUROSCI.2510-13.2013. [PubMed: 24068802]
6. Geoffroy CG, Hilton BJ, Tetzlaff W, and Zheng B (2016). Evidence for an AgeDependent Decline in Axon Regeneration in the Adult Mammalian Central Nervous System. Cell Rep 15, 238–246. 10.1016/j.celrep.2016.03.028. [PubMed: 27050519]
7. Duan X, Qiao M, Bei F, Kim IJ, He Z, and Sanes JR (2015). Subtype-Specific regeneration of retinal ganglion cells following axotomy: Effects of osteopontin and mtor signaling. Neuron 85, 1244–1256. 10.1016/j.neuron.2015.02.017. [PubMed: 25754821]
8. Norsworthy MW, Bei F, Kawaguchi R, Wang Q, Tran NM, Li Y, Brommer B, Zhang Y, Wang C, Sanes JR, et al. (2017). Sox11 Expression Promotes Regeneration of Some Retinal Ganglion Cell Types but Kills Others. Neuron 94, 11121120.e4. 10.1016/J.NEURON.2017.05.035/ATTACHMENT/CA8CC170-DDF9-4AF4B54C-F0DAD909747D/MMC3.PDF.
9. Jaitin DA, Kenigsberg E, Keren-Shaul H, Elefant N, Paul F, Zaretsky I, Mildner A, Cohen N, Jung S, Tanay A, et al. (2014). Massively Parallel Single-Cell RNA-Seq for Marker-Free Decomposition of Tissues into Cell Types. Science 343, 776–779. [PubMed: 24531970]

10. Zheng GXY, Terry JM, Belgrader P, Ryvkin P, Bent ZW, Wilson R, Ziraldo SB, Wheeler TD, McDermott GP, Zhu J, et al. (2017). Massively parallel digital transcriptional profiling of single cells. Nat. Commun 8, 1–12. 10.1038/ncomms14049. [PubMed: 28232747]
11. Tasic B, Yao Z, Graybuck LT, Smith KA, Nguyen TN, Bertagnolli D, Goldy J, Garren E, Economo MN, Viswanathan S, et al. (2018). Shared and distinct transcriptomic cell types across neocortical areas. Nature 563, 72–78. 10.1038/s41586018-0654-5. [PubMed: 30382198]
12. Yao Z, Liu H, Xie F, Fischer S, Adkins RS, Aldridge AI, Ament SA, Bartlett A, Behrens MM, Van den Berge K, et al. (2021). A transcriptomic and epigenomic cell atlas of the mouse primary motor cortex. Nature 598, 103–110. 10.1038/s41586-021-03500-8. [PubMed: 34616066]
13. Keller D, Erö C, and Markram H (2018). Cell densities in the mouse brain: A systematic review. Front. Neuroanat 12, 83. 10.3389/FNANA.2018.00083/BIBTEX. [PubMed: 30405363]
14. van den Brink SC, Sage F, Vértesy Á, Spanjaard B, Peterson-Maduro J, Baron CS, Robin C, and van Oudenaarden A (2017). Single-cell sequencing reveals dissociation-induced gene expression in tissue subpopulations. Nat. Methods 14, 935–936. 10.1038/nmeth.4437. [PubMed: 28960196]
15. Cadwell CR, Palasantza A, Jiang X, Berens P, Deng Q, Yilmaz M, Reimer J, Shen S, Bethge M, Tolias KF, et al. (2015). Electrophysiological, transcriptomic and morphologic profiling of single neurons using Patch-seq. Nat. Biotechnol 34, 1–8. 10.1038/nbt.3445.
16. Fuzik J, Zeisel A, Máté Z, Calvigioni D, Yanagawa Y, Szabó G, Linnarsson S, and Harkany T (2016). integration of electrophysiological recordings with single-cell RNA-seq data identifies neuronal subtypes. Nat. Biotechnol 34. 10.1038/nbt.3443.
17. Gouwens NW, Sorensen SA, Baftizadeh F, Budzillo A, Lee BR, Jarsky T, Alfiler L, Baker K, Barkan E, Berry K, et al. (2020). Integrated Morphoelectric and Transcriptomic Classification of Cortical GABAergic Cells. Cell 183, 935–953.e19. 10.1016/j.cell.2020.09.057. [PubMed: 33186530]
18. Scala F, Kobak D, Bernabucci M, Bernaerts Y, Cadwell CR, Castro JR, Hartmanis L, Jiang X, Laturnus S, Miranda E, et al. (2020). Phenotypic variation of transcriptomic cell types in mouse motor cortex. Nature 598, 144–150. 10.1038/s41586-020-2907-3. [PubMed: 33184512]
19. Kim J.M. “Hugo,” Camarena A, Walker C, Lin MY, Wolseley V, Souaiaia T, Thornton M, Grubbs B, Chow RH, Evgrafov OV, et al. (2020). Robust RNA-Seq of aRNA-amplified single cell material collected by patch clamp. Sci. Rep 10, 1979. 10.1038/s41598-020-58715-y. [PubMed: 32029778]
20. Sun F, Park KK, Belin S, Wang D, Lu T, Chen G, Zhang K, Yeung C, Feng G, Yankner BA, et al. (2011). Sustained axon regeneration induced by co-deletion of PTEN and SOCS3. Nature 480, 372–375. 10.1038/nature10594. [PubMed: 22056987]
21. Jin D, Liu Y, Sun F, Wang X, Liu X, and He Z (2015). Restoration of skilled locomotion by sprouting corticospinal axons induced by co-deletion of PTEN and SOCS3. Nat. Commun 6, 1–12. 10.1038/ncomms9074.
22. Madisen L, Zwingman TA, Sunkin SM, Oh SW, Zariwala HA, Gu H, Ng LL, Palmiter RD, Hawrylycz MJ, Jones AR, et al. (2010). A robust and high-throughput Cre reporting and characterization system for the whole mouse brain. Nat. Neurosci 13, 133–140. 10.1038/nn.2467. [PubMed: 20023653]
23. Aran D, Looney AP, Liu L, Wu E, Fong V, Hsu A, Chak S, Naikawadi RP, Wolters PJ, Abate AR, et al. (2019). Reference-based analysis of lung single-cell sequencing reveals a transitional profibrotic macrophage. Nat. Immunol 20, 163–172. 10.1038/s41590-018-0276-y. [PubMed: 30643263]
24. Kiselev VY, Andrews TS, and Hemberg M (2019). Challenges in unsupervised clustering of single-cell RNA-seq data. Nat. Rev. Genet 20, 273–282. 10.1038/s41576018-0088-9. [PubMed: 30617341]
25. Pliner HA, Shendure J, and Trapnell C (2019). Supervised classification enables rapid annotation of cell atlases. Nat. Methods 16, 983–986. 10.1038/s41592-019-0535-3. [PubMed: 31501545]
26. Canty AJ, Huang L, Jackson JS, Little GE, Knott G, Maco B, and De Paola V (2013). In-vivo single neuron axotomy triggers axon regeneration to restore synaptic density in specific cortical circuits. Nat. Commun 4, 1–10. 10.1038/ncomms3038.

27. Okaty BW, Sturrock N, Lozoya YE, Chang Y, Senft RA, Lyon KA, Alekseyenko OV, and Dymecki SM (2020). A single-cell transcriptomic and anatomic atlas of mouse dorsal raphe Pet1 neurons. Elife 9, 1–44. 10.7554/eLife.55523.
28. Jin Y, Dougherty SE, Wood K, Sun L, Cudmore RH, Abdalla A, Kannan G, Pletnikov M, Hashemi P, and Linden DJ (2016). Regrowth of serotonin axons in the adult mouse brain following injury. Neuron 91, 748. 10.1016/J.NEURON.2016.07.024. [PubMed: 27499084]
29. Shekhar K, Whitney IE, Butrus S, Peng YR, and Sanes JR (2022). Diversification of multipotential postmitotic mouse retinal ganglion cell precursors into discrete types. Elife 11. 10.7554/ELIFE.73809.
30. Tran NM, Shekhar K, Whitney IE, Jacobi A, Benhar I, Hong G, Yan W, Adiconis X, Arnold ME, Lee JM, et al. (2019). Single-Cell Profiles of Retinal Ganglion Cells Differing in Resilience to Injury Reveal Neuroprotective Genes. Neuron 104, 1039–1055. 10.1016/j.neuron.2019.11.006. [PubMed: 31784286]
31. Goldberg JL, Klassen MP, Hua Y, and Barres BA (2002). Amacrine-signaled loss of intrinsic axon growth ability by retinal ganglion cells. Science 296, 1860–1864. 10.1126/SCIENCE.1068428/ASSET/37314A39-ED04-4CE1-9A67-16479AB2D6AD/ASSETS/GRAPHIC/SE2220567004.JPEG. [PubMed: 12052959]
32. La Manno G, Gyllborg D, Codeluppi S, Nishimura K, Salto C, Zeisel A, Borm LE, Stott SRW, Toledo EM, Villaescusa JC, et al. (2016). Molecular Diversity of Midbrain Development in Mouse, Human, and Stem Cells. Cell 167, 566–580.e19. 10.1016/J.CELL.2016.09.027/ATTACHMENT/9B9F4EBE-66CF-4A26-A38E-2793511300BB/MMC2.XLSX. [PubMed: 27716510]
33. Bhattacherjee A, Djekidel MN, Chen R, Chen W, Tuesta LM, and Zhang Y (2019). Cell type-specific transcriptional programs in mouse prefrontal cortex during adolescence and addiction. Nat. Commun 10, 1–18. 10.1038/s41467-019-12054-3. [PubMed: 30602773]
34. Delile J, Rayon T, Melchionda M, Edwards A, Briscoe J, and Sagner A (2019). Single cell transcriptomics reveals spatial and temporal dynamics of gene expression in the developing mouse spinal cord. Dev 146. 10.1242/DEV.173807/264914/AM/SINGLECELL-TRANSCRIPTOMICS-REVEALS-SPATIAL-AND.
35. Hayashi M, Hinckley CA, Driscoll SP, Moore NJ, Levine AJ, Hilde KL, Sharma K, and Pfaff SL (2018). Graded Arrays of Spinal and Supraspinal V2a Interneuron Subtypes Underlie Forelimb and Hindlimb Motor Control. Neuron 97, 869–884.e5. [PubMed: 29398364]
36. Milich LM, Choi JS, Ryan C, Cerqueira SR, Benavides S, Yahn SL, Tsoulfas P, and Lee JK (2021). Single-cell analysis of the cellular heterogeneity and interactions in the injured mouse spinal cord. J. Exp. Med 218. 10.1084/jem.20210040.
37. Zeisel A, Hochgerner H, Lönnerberg P, Johnsson A, Memic F, van der Zwan J, Häring M, Braun E, Borm LE, La Manno G, et al. (2018). Molecular Architecture of the Mouse Nervous System. Cell 174, 999–1014.e22. 10.1016/j.cell.2018.06.021. [PubMed: 30096314]
38. Zeisel A, Muñoz-Manchado AB, Codeluppi S, Lönnerberg P, La Manno G, Juréus A, Marques S, Munguba H, He L, Betsholtz C, et al. (2015). Cell types in the mouse cortex and hippocampus revealed by single-cell RNA-seq. Science 347.
39. Avraham O, Deng PY, Jones S, Kuruvilla R, Semenkovich CF, Klyachko VA, and Cavalli V (2020). Satellite glial cells promote regenerative growth in sensory neurons. Nat. Commun 11, 1–17. 10.1038/s41467-020-18642-y. [PubMed: 31911652]
40. Usoskin D, Furlan A, Islam S, Abdo H, Lönnerberg P, Lou D, Hjerling-Leffler J, Haeggström J, Kharchenko O, Kharchenko PV, et al. (2014). Unbiased classification of sensory neuron types by large-scale single-cell RNA sequencing. Nat. Neurosci 18, 145–153. 10.1038/nn.3881. [PubMed: 25420068]
41. Avraham O, Feng R, Ewan EE, and Rustenhoven J (2021). Profiling sensory neuron microenvironment after peripheral and central axon injury reveals key pathways for neural repair. Elife 10, e68457. [PubMed: 34586065]
42. Jessa S, Blanchet-Cohen A, Krug B, Vladoiu M, Coutelier M, Faury D, Poreau B, De Jay N, Hébert S, Monlong J, et al. (2019). Stalled developmental programs at the root of pediatric brain tumors. Nat. Genet 51, 1702–1713. 10.1038/s41588-019-0531-7. [PubMed: 31768071]

43. Romanov RA, Zeisel A, Bakker J, Girach F, Hellysaz A, Tomer R, Alpár A, Mulder J, Clotman F, Keimpema E, et al. (2016). Molecular interrogation of hypothalamic organization reveals distinct dopamine neuronal subtypes. Nat. Neurosci 20, 176–188. 10.1038/nn.4462. [PubMed: 27991900]
44. Campbell JN, Macosko EZ, Fenselau H, Pers TH, Lyubetskaya A, Tenen D, Goldman M, Verstegen AMJ, Resch JM, McCarroll SA, et al. (2017). A Molecular Census of Arcuate Hypothalamus and Median Eminence Cell Types. Nat. Neurosci 20, 484. 10.1038/NN.4495. [PubMed: 28166221]
45. Liau ES, Jin S, Chen YC, Liu WS, Calon M, Nedelec S, Nie Q, and Chen JA (2023). Single-cell transcriptomic analysis reveals diversity within mammalian spinal motor neurons. Nat. Commun 14, 46. 10.1038/s41467-022-35574-x. [PubMed: 36596814]
46. Chen R, Wu X, Jiang L, and Zhang Y (2017). Single-Cell RNA-Seq Reveals Hypothalamic Cell Diversity. Cell Rep 18, 3227–3241. 10.1016/j.celrep.2017.03.004. [PubMed: 28355573]
47. Tasic B, Menon V, Nguyen TN, Kim TK, Jarsky T, Yao Z, Levi B, Gray LT, Sorensen SA, Dolbeare T, et al. (2016). Adult mouse cortical cell taxonomy revealed by single cell transcriptomics. Nat. Neurosci 19, 335–346. 10.1038/nn.4216. [PubMed: 26727548]
48. Peng J, Sheng AL, Xiao Q, Shen L, Ju XC, Zhang M, He ST, Wu C, and Luo ZG (2019). Single-cell transcriptomes reveal molecular specializations of neuronal cell types in the developing cerebellum. J. Mol. Cell Biol 11, 636–648. 10.1093/JMCB/MJY089.
49. Fenrich KK, and Rose PK (2009). Spinal Interneuron Axons Spontaneously Regenerate after Spinal Cord Injury in the Adult Feline. J. Neurosci 29, 12145–12158. 10.1523/JNEUROSCI.0897-09.2009. [PubMed: 19793972]
50. Poplawski GHD, Kawaguchi R, Van Niekerk E, Lu P, Mehta N, Canete P, Lie R, Dragatsis I, Meves JM, Zheng B, et al. (2020). Injured adult neurons regress to an embryonic transcriptional growth state. Nature 581, 77–82. 10.1038/s41586-020-2200-5. [PubMed: 32376949]
51. Jacobi A, Tran NM, Yan W, Benhar I, Tian F, Schaffer R, He Z, and Sanes JR (2022). Overlapping transcriptional programs promote survival and axonal regeneration of injured retinal ganglion cells. Neuron 110, 2625–2645.e7. 10.1016/J.NEURON.2022.06.002. [PubMed: 35767994]
52. Matson KJE, Russ DE, Kathe C, Hua I, Maric D, Ding Y, Krynitsky J, Pursley R, Sathyamurthy A, Squair JW, et al. (2022). Single cell atlas of spinal cord injury in mice reveals a pro-regenerative signature in spinocerebellar neurons. Nat. Commun 13, 1–16. 10.1038/s41467-022-33184-1. [PubMed: 34983933]
53. Sathyamurthy A, Johnson KR, Matson KJE, Dobrott CI, Li L, Ryba AR, Bergman TB, Kelly MC, Kelley MW, and Levine AJ (2018). Massively Parallel Single Nucleus Transcriptional Profiling Defines Spinal Cord Neurons and Their Activity during Behavior. Cell Rep 22, 2216–2225. [PubMed: 29466745]
54. Hu P, Fabyanic E, Kwon DY, Tang S, Zhou Z, and Wu H (2017). Dissecting CellType Composition and Activity-Dependent Transcriptional State in Mammalian Brains by Massively Parallel Single-Nucleus RNA-Seq. Mol. Cell 68, 1006–1015.e7. 10.1016/J.MOLCEL.2017.11.017/ATTACHMENT/05989D28-8A2A-44AA-B139-E16877EBEC6E/MMC5.MP4. [PubMed: 29220646]
55. Beine Z, Wang Z, Tsoulfas P, and Blackmore MG (2022). Single nuclei analyses reveal transcriptional profiles and marker genes for diverse supraspinal populations. J. Neurosci 42, 8780–8794. 10.1523/jneurosci.1197-22.2022. [PubMed: 36202615]
56. Slyper M, Porter CBM, Ashenberg O, Waldman J, Drokhlyansky E, Wakiro I, Smillie C, Smith-Rosario G, Wu J, Dionne D, et al. (2020). A single-cell and singlenucleus RNA-Seq toolbox for fresh and frozen human tumors. Nat. Med 26, 792–802. 10.1038/s41591-020-0844-1. [PubMed: 32405060]
57. Xu X, Cui Y, Li C, Wang Y, Cheng J, Chen S, Sun J, Ren J, Yao X, Gao J, et al. (2021). SETD3 Downregulation Mediates PTEN Upregulation-Induced Ischemic Neuronal Death Through Suppression of Actin Polymerization and Mitochondrial Function. Mol. Neurobiol 58, 4906–4920. 10.1007/S12035-021-02459-X/FIGURES/9. [PubMed: 34218417]
58. Kryszczuk M, and Kowalczuk O (2022). Significance of NRF2 in physiological and pathological conditions an comprehensive review. Arch. Biochem. Biophys 730, 109417. 10.1016/J.ABB.2022.109417. [PubMed: 36202215]

59. Baldelli S, Aquilano K, and Ciriolo MR (2013). Punctum on two different transcription factors regulated by PGC-1α: Nuclear factor erythroid-derived 2-like 2 and nuclear respiratory factor 2. Biochim. Biophys. Acta - Gen. Subj 1830, 4137–4146. 10.1016/J.BBAGEN.2013.04.006.
60. Rius-Pérez S, Torres-Cuevas I, Millán I, Ortega ÁL, Pérez S, and Sandhu MA (2020). PGC-1 α, Inflammation, and Oxidative Stress: An Integrative View in Metabolism. Oxid. Med. Cell. Longev 2020. 10.1155/2020/1452696.
61. Miao L, Yang L, Huang H, Liang F, Ling C, and Hu Y (2016). MTORC1 is necessary but mTORC2 and GSK3β are inhibitory for AKT3-induced axon regeneration in the central nervous system. Elife 5. 10.7554/ELIFE.14908.
62. Kuo TY, Hong CJ, Chien HL, and Hsueh YP (2010). X-linked mental retardation gene CASK interacts with Bcl11A/CTIP1 and regulates axon branching and outgrowth. J. Neurosci. Res 88, 2364–2373. 10.1002/JNR.22407. [PubMed: 20623620]
63. Friedson B, Cooper KF, Guaragnella N, Krisko A, and Outeiro TF (2021). Cdk8 Kinase Module: A Mediator of Life and Death Decisions in Times of Stress. Microorganisms 9, 2152. 10.3390/MICROORGANISMS9102152. [PubMed: 34683473]
64. Gumireddy K, Li A, Gimotty PA, Klein-Szanto AJ, Showe LC, Katsaros D, Coukos G, Zhang L, and Huang Q (2009). KLF17 is a negative regulator of epithelial–mesenchymal transition and metastasis in breast cancer. Nat. Cell Biol 11, 1297–1304. 10.1038/ncb1974. [PubMed: 19801974]
65. Moore DL, Blackmore MG, Hu Y, Kaestner KH, Bixby JL, Lemmon VP, and Goldberg JL (2009). KLF family members regulate intrinsic axon regeneration ability. Science 326, 298–301. 10.1126/SCIENCE.1175737/SUPPL_FILE/MOORE.SOM.PDF. [PubMed: 19815778]
66. Cargnin F, Kwon JS, Katzman S, Chen B, Lee JW, and Lee SK (2018). FOXG1 Orchestrates Neocortical Organization and Cortico-Cortical Connections. Neuron 100, 1083–1096.e5. 10.1016/j.neuron.2018.10.016. [PubMed: 30392794]
67. Saikia JM, Chavez-Martinez CL, Kim ND, Allibhoy S, Kim HJ, Simonyan L, Smadi S, Tsai KM, Romaus-Sanjurjo D, Jin Y, et al. (2022). A Critical Role for DLK and LZK in Axonal Repair in the Mammalian Spinal Cord. J. Neurosci 42, 3716–3732. 10.1523/JNEUROSCI.2495-21.2022. [PubMed: 35361703]
68. Lee JK, Geoffroy CG, Chan AF, Tolentino KE, Crawford MJ, Leal MA, Kang B, and Zheng B (2010). Assessing Spinal Axon Regeneration and Sprouting in Nogo-, MAG-, and OMgp-Deficient Mice. Neuron 66, 663–670. 10.1016/J.NEURON.2010.05.002. [PubMed: 20547125]
69. Ohtake Y, Park D, Abdul-Muneer PM, Li H, Xu B, Sharma K, Smith GM, Selzer ME, and Li S (2014). The effect of systemic PTEN antagonist peptides on axon growth and functional recovery after spinal cord injury. Biomaterials 35, 4610–4626. 10.1016/j.biomaterials.2014.02.037. [PubMed: 24630093]
70. Romaus-Sanjurjo D, Saikia JM, Kim HJ, Tsai KM, Le GQ, and Zheng B (2022). Overexpressing eukaryotic elongation factor 1 alpha (eEF1A) proteins to promote corticospinal axon repair after injury. Cell Death Discov 8, 1–13. 10.1038/s41420-02201186-z. [PubMed: 35013145]
71. Belin S, Nawabi H, Wang C, Tang S, Latremoliere A, Warren P, Schorle H, Uncu C, Woolf CJ, He Z, et al. (2015). Injury-Induced Decline of Intrinsic Regenerative Ability Revealed by Quantitative Proteomics. Neuron 86, 1000–1014. 10.1016/j.neuron.2015.03.060. [PubMed: 25937169]
72. Özdinler PH, and Macklis JD (2006). IGF-I specifically enhances axon outgrowth of corticospinal motor neurons. Nat. Neurosci 9, 1371–1381. 10.1038/nn1789. [PubMed: 17057708]
73. Ngo V, and Duennwald ML (2022). Nrf2 and Oxidative Stress: A General Overview of Mechanisms and Implications in Human Disease Antioxidants (Basel, Switzerland) 11. 10.3390/antiox11122345.
74. Schmidlin CJ, Dodson MB, Madhavan L, and Zhang DD (2019). Redox Regulation by NRF2 in Aging and Disease. Free Radic. Biol. Med 134, 702. 10.1016/J.FREERADBIOMED.2019.01.016. [PubMed: 30654017]
75. Hervera A, Virgiliis F. De, Palmisano I, Zhou L, Tantardini E, Kong G, Hutson T, Danzi MC, Perry RB, Santos CXC, et al. (2018). regeneration through the release of exosomal NADPH oxidase 2 complexes into injured axons. Nat. Cell Biol 20. 10.1038/s41556-018-0039-x.

76. Sanchis-Gomar F, Garcia-Gimenez J, Gomez-Cabrera M, and Pallardo F (2014). Mitochondrial Biogenesis in Health and Disease. Molecular and Therapeutic Approaches. Curr. Pharm. Des 20, 5619–5633. 10.2174/1381612820666140306095106. [PubMed: 24606801]
77. Ryoo I. geun, and Kwak MK (2018). Regulatory crosstalk between the oxidative stressrelated transcription factor Nfe2l2/Nrf2 and mitochondria. Toxicol. Appl. Pharmacol 359, 24–33. 10.1016/J.TAAP.2018.09.014. [PubMed: 30236989]
78. Hyttinen J, Blasiak J, Tavi P, and Kaarniranta K (2021). Therapeutic potential of PGC-1α in age-related macular degeneration (AMD) – the involvement of mitochondrial quality control, autophagy, and antioxidant response. Expert Opin. Ther. Targets 25, 773–785. 10.1080/14728222.2021.1991913. [PubMed: 34637373]
79. Gureev AP, Shaforostova EA, and Popov VN (2019). Regulation of mitochondrial biogenesis as a way for active longevity: Interaction between the Nrf2 and PGC-1α signaling pathways. Front. Genet 10, 1–12. 10.3389/fgene.2019.00435. [PubMed: 30804975]
80. Han Q, Xie Y, Ordaz JD, Huh AJ, Huang N, Wu W, Liu N, Chamberlain KA, Sheng ZH, and Xu XM (2020). Restoring Cellular Energetics Promotes Axonal Regeneration and Functional Recovery after Spinal Cord Injury. Cell Metab 31, 623–641.e8. 10.1016/j.cmet.2020.02.002. [PubMed: 32130884]
81. Huang N, Li S, Xie Y, Han Q, Xu XM, and Sheng ZH (2021). Reprogramming an energetic AKT-PAK5 axis boosts axon energy supply and facilitates neuron survival and regeneration after injury and ischemia. Curr. Biol 31, 3098–3114.e7. 10.1016/J.CUB.2021.04.079. [PubMed: 34087103]
82. Cartoni R, Norsworthy MW, Bei F, Wang C, Li S, Zhang Y, Gabel CV, Schwarz TL, and He Z (2016). The Mammalian-Specific Protein Armcx1 Regulates Mitochondrial Transport during Axon Regeneration. Neuron 92, 1294–1307. 10.1016/j.neuron.2016.10.060. [PubMed: 28009275]
83. Al-Khindi T, Sherman MB, Kodama T, Gopal P, Pan Z, Kiraly JK, Zhang H, Goff LA, du Lac S, and Kolodkin AL (2022). The transcription factor Tbx5 regulates direction-selective retinal ganglion cell development and image stabilization. Curr. Biol 32, 4286–4298.e5. 10.1016/j.cub.2022.07.064. [PubMed: 35998637]
84. Li J, and Eberwine J (2018). The successes and future prospects of the linear antisense RNA amplification methodology. Nat. Protoc 13, 811–818. 10.1038/nprot.2018.011. [PubMed: 29599441]
85. Geoffroy CG, Meves JM, Kim HJM, Romaus-Sanjurjo D, Sutherland TC, Li JJ, Suen J, Sanchez JJ, and Zheng B (2022). Targeting PTEN but not SOCS3 resists an age-dependent decline in promoting axon sprouting. iScience 25, 105383. 10.1016/J.ISCI.2022.105383. [PubMed: 36339257]
86. Dobin A, Davis CA, Schlesinger F, Drenkow J, Zaleski C, Jha S, Batut P, Chaisson M, and Gingeras TR (2013). STAR: Ultrafast universal RNA-seq aligner. Bioinformatics 29, 15–21. 10.1093/bioinformatics/bts635. [PubMed: 23104886]
87. Li H, Handsaker B, Wysoker A, Fennell T, Ruan J, Homer N, Marth G, Abecasis G, and Durbin R (2009). The Sequence Alignment/Map format and SAMtools. Bioinformatics 25, 2078–2079. 10.1093/bioinformatics/btp352. [PubMed: 19505943]
88. Putri GH, Anders S, Pyl PT, Pimanda JE, and Zanini F (2022). Analysing highthroughput sequencing data in Python with HTSeq 2.0. Bioinformatics 38, 2943–2945. 10.1093/bioinformatics/btac166. [PubMed: 35561197]
89. Love MI, Huber W, and Anders S (2014). Moderated estimation of fold change and dispersion for RNA-seq data with DESeq2. Genome Biol 15, 1–21. 10.1186/s13059-014-0550-8.
90. Robinson MD, McCarthy DJ, and Smyth GK (2009). edgeR: A Bioconductor package for differential expression analysis of digital gene expression data. Bioinformatics 26, 139–140. 10.1093/bioinformatics/btp616. [PubMed: 19910308]
91. Butler A, Hoffman P, Smibert P, Papalexi E, and Satija R (2018). Integrating singlecell transcriptomic data across different conditions, technologies, and species. Nat. Biotechnol 36, 411–420. 10.1038/nbt.4096. [PubMed: 29608179]
92. McCarthy DJ, Campbell KR, Lun ATL, and Wills QF (2017). Scater: Preprocessing, quality control, normalization and visualization of single-cell RNA-seq data in R. Bioinformatics 33, 1179–1186. 10.1093/bioinformatics/btw777. [PubMed: 28088763]

93. Ashburner M, Ball CA, Blake JA, Botstein D, Butler H, Cherry JM, Davis AP, Dolinski K, Dwight SS, Eppig JT, et al. (2000). Gene Ontology: tool for the unification of biology. Nat. Genet 2000 251 25, 25–29. 10.1038/75556. [PubMed: 10802651]

94. Schneider CA, Rasband WS, and Eliceiri KW (2012). NIH Image to ImageJ: 25 years of image analysis. Nat. Methods 9, 671–675. 10.1038/nmeth.2089. [PubMed: 22930834]

95. University of California, S.D.S. (2022). San Diego Supercomputer Center (2022): Triton Shared Computing Cluster 10.57873/T34W2R.

96. Risso D, Cole M, Lun A, O'Callaghan A, Preussner J, Soneson C, Orjuela S, Bunis D, and Malfait M (2022). scRNAseq: Collection of Public Single-Cell RNA-Seq Datasets. R Packag. version 2.10.0

97. Satija R, Farrell JA, Gennert D, Schier AF, and Regev A (2015). Spatial reconstruction of single-cell gene expression data. Nat. Biotechnol 33, 495–502. 10.1038/nbt.3192. [PubMed: 25867923]

Highlights

- Applying Garnett to deep scRNA-Seq of CST neurons led to Regeneration Classifier
- Regeneration Classifier predicts regenerative potential of diverse neuronal types
- Network analyses implicate antioxidant response and mitochondrial biogenesis
- Deleting antioxidant response gene *NFE2L2* blocks CST axon regeneration

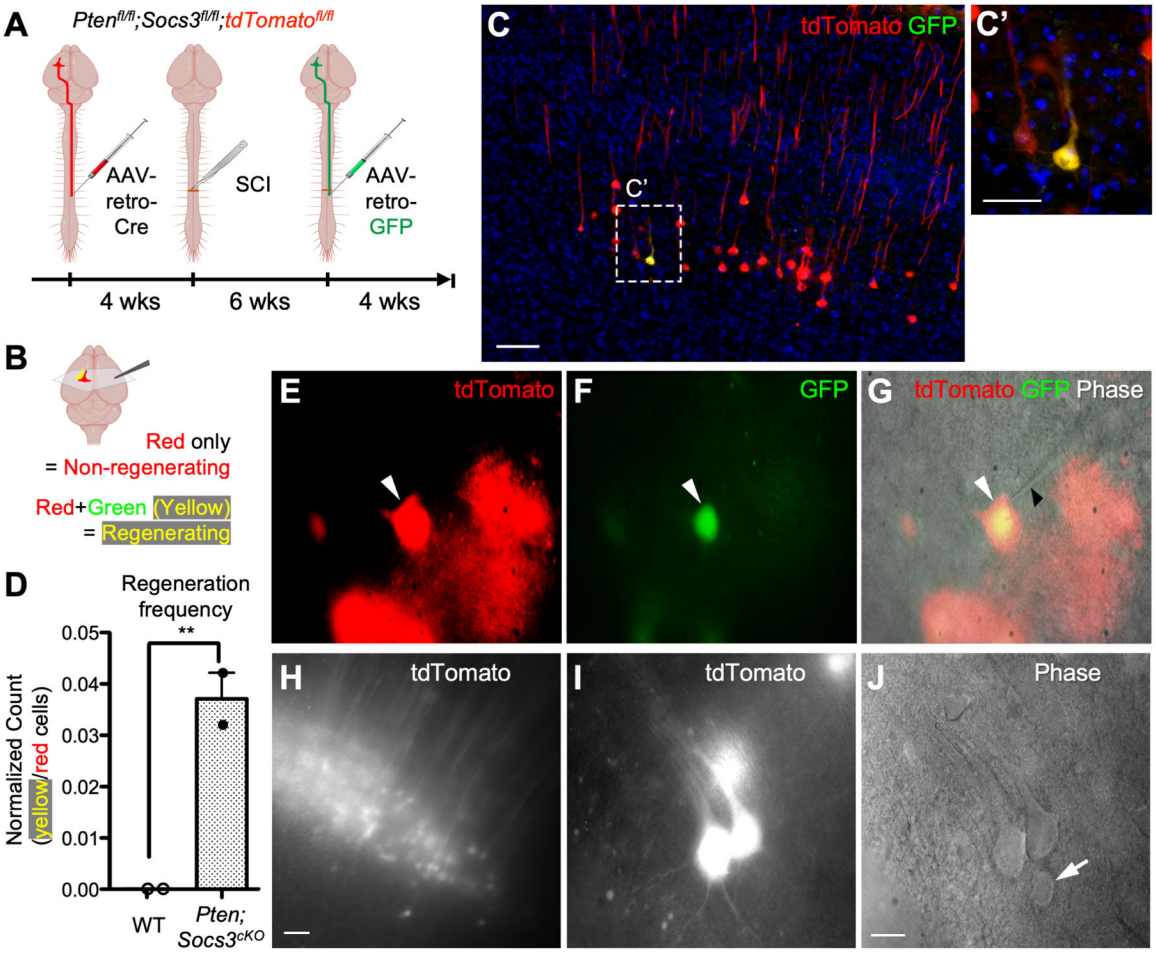

Figure 1. Patch-based deep scRNA sequencing of rate regenerating CST neurons following *PTEN* and *SOCS3* deletion.

(A) Surgical timeline. SCI, dorsal hemisection spinal cord injury. (B) With dual retrograde AAV tracing with one virus before and another after injury, regenerating CST neurons would be labeled in both green and red (yellow) while non-regenerating neurons will be labeled in red only. (C) Representative immunohistochemical image of retrograde AAV traced CST neurons in cortical layer 5 illustrating the typically low incidence of regeneration by CST neurons (red + green = yellow) following *PTEN* and *SOCS3* deletion. Scale Bar = 100 μm; 20 μm (c' high mag). (D) Quantification of regeneration frequency as the number of regenerating (red + green = yellow) neurons normalized against the total number of retrogradely labeled (red) neurons in wild-type (WT) and *Pten;Socs3* conditional knockout (cKO) mice. N = 2 per genotype. **p < 0.01, one-tailed unpaired *t*-test. Dots represent individual mice. Error bar = SEM. (E-G) Patch clamp collection of a regenerating CST neuron marked by both tdTomato and GFP (white arrowhead) from an acute brain slice. In (G), tdTomato, GFP channels are merged with phase contrast taken from a patch rig at high magnification, where black arrowhead marks the patch pipette approaching the doubly labeled neuron. (H) Many tdTomato fluorescent CST neurons in the area of interest can be seen at low magnification in the brain slice. (I,J) tdTomato positive neurons neighboring a

tdTomato negative cell (white arrow). Scale Bar = 100 μm (H), 20 μm (E-G, I, J). See also Figure S1.

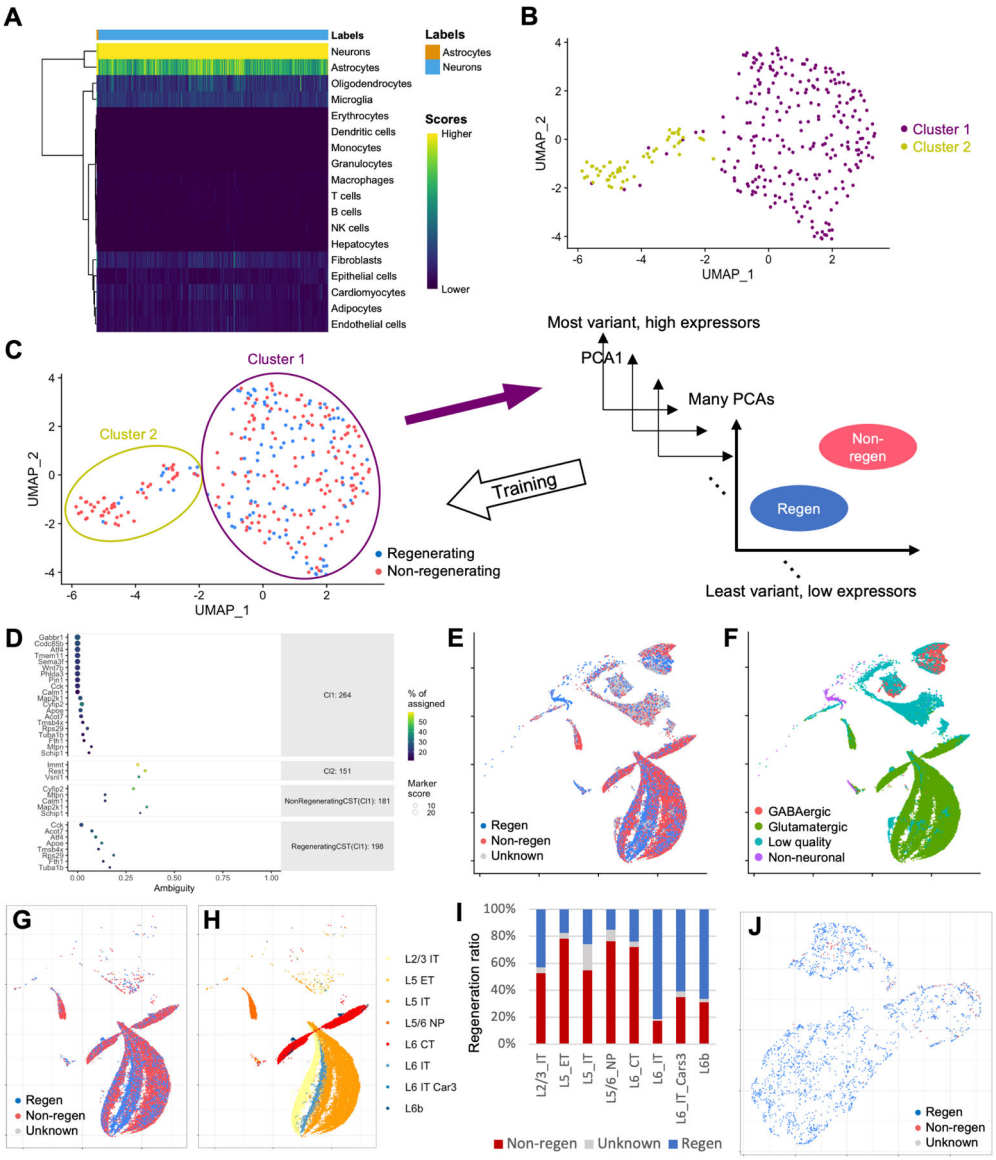

Figure 2. Single cell clustering analysis on Patch-Seq'ed corticospinal neurons.

(A) Cell type analysis using SingleR. The most expressed markers were neuronal markers. The vast majority of cells were classified as neurons. (B) UMAP representation of unsupervised single cell clustering by Seurat. (C) Developing Regeneration Classifier (RC) with machine learning of single cell data with Garnett. (D) Main Markers used as initial categorization of Regeneration Classifier and ambiguity testing of regenerating/non-regenerating markers on all clusters (Cluster 1,2 and Regen/Non-regen). (E-I) Applying RC to a published dataset on neurons from the mouse primary motor cortex (Yao et al., 2021) illustrates regenerative heterogeneity. (E) UMAP plot after applying RC to all cells. (F) Original UMAP plot of all cells. (G) UMAP plot after applying RC to glutamatergic neurons only. (H) Original UMAP showing sub-classification of glutamatergic neurons based on cortical layers and axonal projections. ET, extratelencephalically projecting; IT, intratelencephalically projecting; NP, near-projecting; CT, corticothalamic. (I) Regeneration

ratio plot (including regenerating, non-regenerating and unknown) for different subtypes of glutamatergic neurons after applying the RC. (J) Applying RC to neurons from raphe nuclei (Okaty et al., 2020). Note most neurons from raphe nuclei are classified as regenerators.

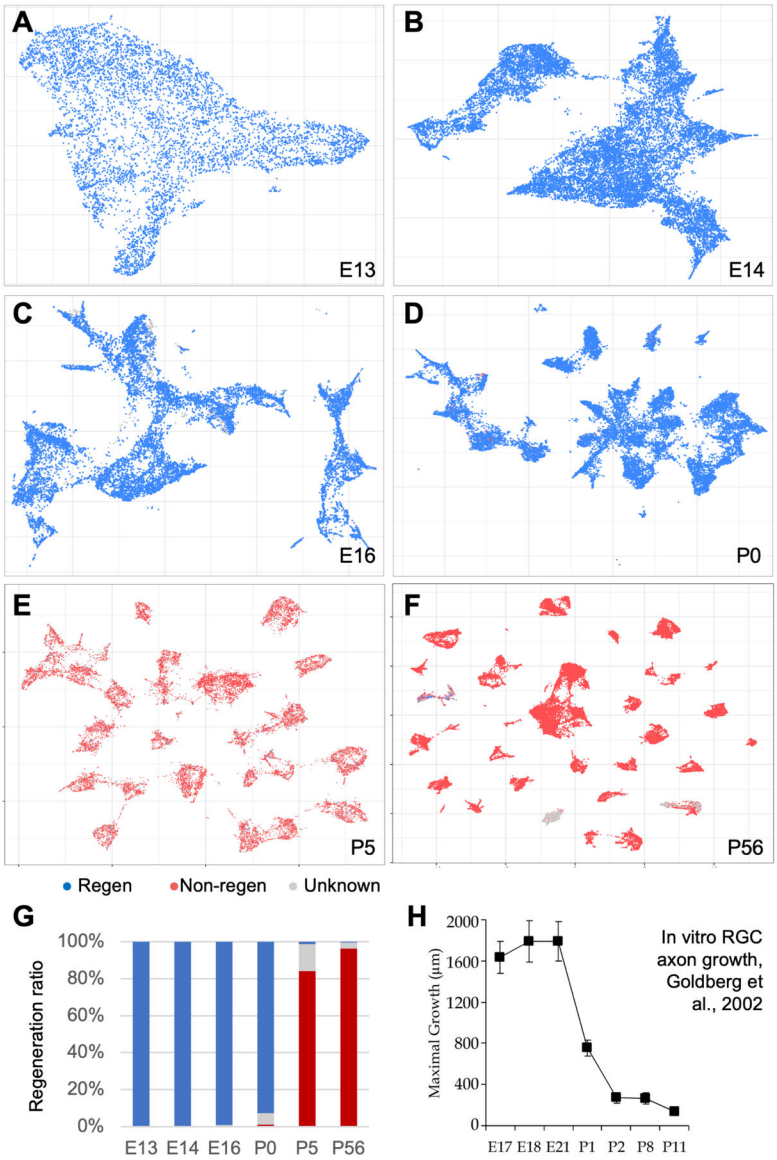

Figure 3. Applying Regeneration Classifier to retinal ganglion cells (RGCs) across developmental stages reveals transcriptomic basis for the precipitous decline of intrinsic axon growth ability of RGCs at an early postnatal age.

(A-F) UMAP plots of scRNA-Seq data on RGCs from different developmental stages in mice, color coded for regeneration classifications. (G) Regeneration ratio plot based on the regeneration classifications. Sc-RNA Seq data source: E13 – P5, Shekhar et al. 2022; P56, Tran et al., 2019 (both papers were published by the same research team). (H) Intrinsic axon growth ability of in vitro cultured RGCs isolated from rats of different ages reported by Goldberg et al., 2002. Note the striking resemblance on the developmental decline postnatally in (G) and (H).

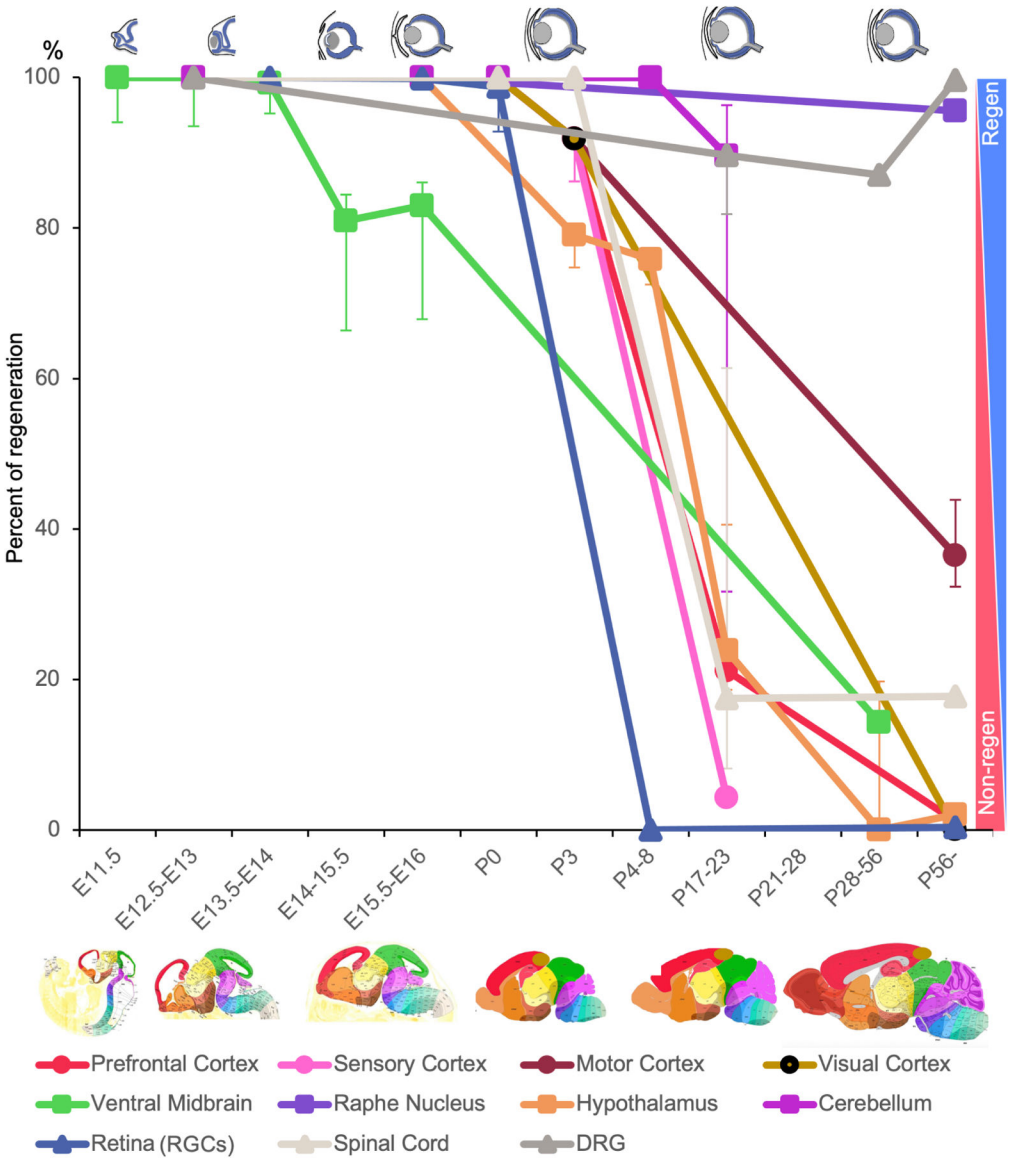

Figure 4. Applying Regeneration Classifier to published scRNA-Seq data generates cell type- and developmental stage-appropriate classifications.

Percent of regeneration is calculated as the number of regenerating neurons over the sum of regenerating and nonregenerating neurons, with the assumption that unknowns are in the same ratio as regenerating and non-regenerating neurons for the first approximation. Error bars mark the extreme cases where all the unknowns are non-regenerating at the low end or regenerating at the high end. There is a general trend for development-dependent decline in regeneration potential, with some neuronal populations being more resistant to this decline such as neurons in DRGs (dorsal root ganglia) and the raphe nuclei. For prefrontal, sensory, motor and visual cortices, the earlier data points were from the forebrain; for raphe nucleus, hypothalamus and cerebellum, the earlier data points were from the hindbrain. ScRNA-Seq data source: Prefrontal Cortex: Jessa et al., 2019 (E12.5-P3/Forebrain), Bhattacherjee et al 2019 (P21, P28–56); Sensory Cortex: Jessa et al., 2019 (E12.5-P3/Forebrain), Zeisel et al. 2015 (P21); Motor Cortex: Jessa et al., 2019 (E12.5-P3/Forebrain), Yao et al. 2022 (P56);

Visual Cortex: Jessa et al., 2019 (E12.5-P3/Forebrain), Tasic et al. 2015 (P56); Ventral Midbrain: La Manno et al., 2016 (E11.5-E18.5, P28–56); Raphe Nucleus: Jessa et al., 2019 (E12.5-E16/Hindbrain), Okaty et al. 2020 (P35–70); Hypothalamus: Jessa et al., 2019 (E12.5-P6 /Hindbrain), Romanov et al. 2017 (Juvenile), Campbell et al., 2017 (Adult), Chen et al., 2017 (P56); Cerebellum: Jessa et al. 2019 E12.5-E16/Hindbrain), Peng et al., 2019 (P0,P8), Zeisel et al., 2018 (P20); Retina (RGCs): Shekhar et al. 2022 (E13-P5), Tran et al., 2019 (P56); Spinal cord: Delile et al., 2019 (E9.5–13.5), Liau et al., 2023 (E13.5), Hayshi et al., 2018 (P0–3), Zeisel et al., 2018 (P20), Hairing et al., 2018 (P21–28), Milich et al., 2020 (Adult); DRG (dorsal root ganglia): Zeisel et al., 2018 (P20), Zeisel et al., 2018 (P20), Usoskin et al., 2015 (P42–56), Avraham et al., 2020 (P56-). Note that DRG neurons exhibit a dip and then recovers likely due to the small sample size and/or the use of older technologies in Zeisel et al., 2018 and Usoskin et al., 2015. Retina diagrams (top graph): modified from Beby and Lamonerie, 2013; brain diagrams (bottom graph): modified from Thompson et al., 2014. See also Figures S2–S4.

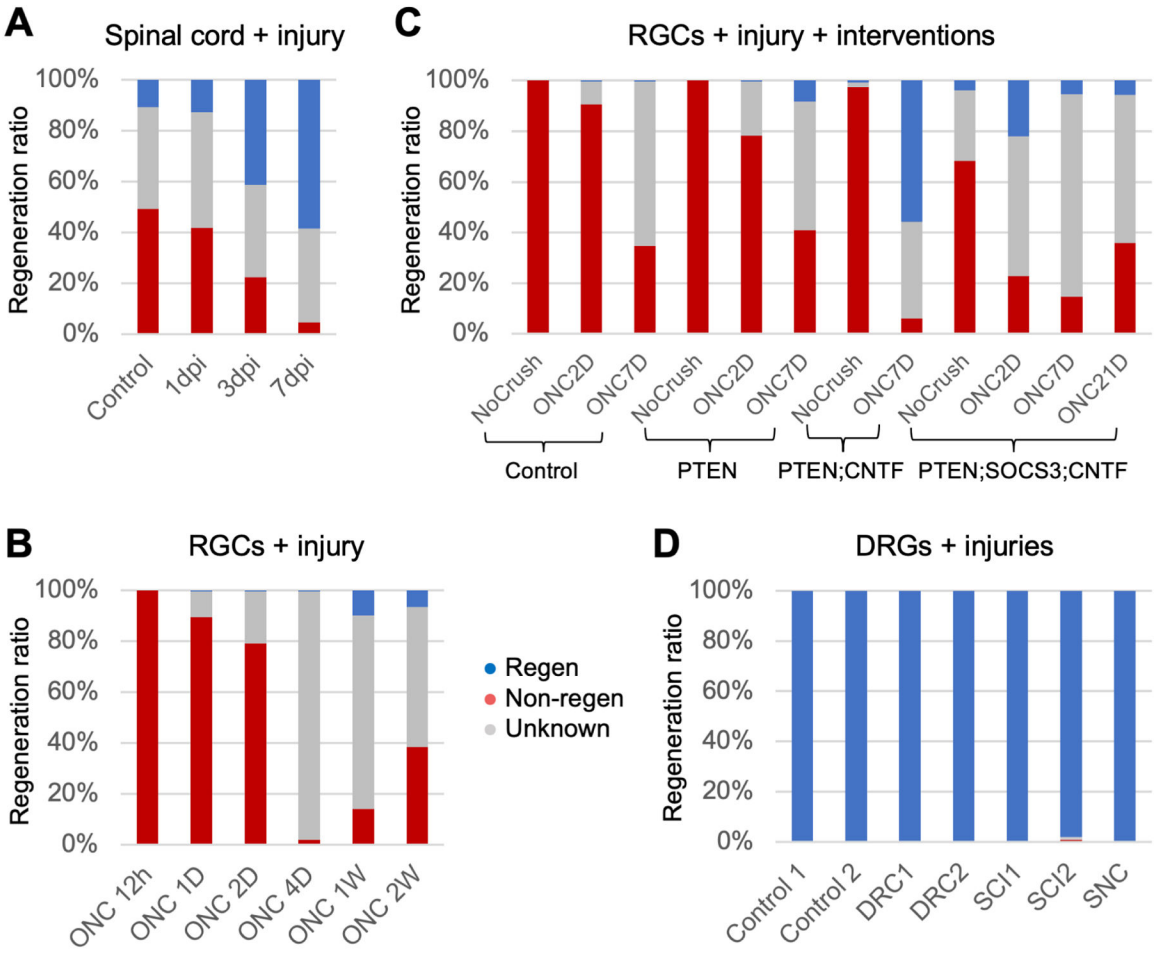

Figure 5. Applying Regeneration Classifier to neurons after injury reveals neuron typespecific responses.

(A-D) Regeneration ratio plots on scRNA-Seq data from spinal neurons around a spinal cord injury site (A), retinal ganglion cells (RGCs) after optic nerve crush without molecular interventions (B), RGCs after optic nerve crush with molecular interventions including PTEN/SOCS3 conditional knockout, and/or CNTF overexpression (C), dorsal root ganglion (DRG) neurons after various injuries (D). Note that the control RGC profile especially at 7 days after optic nerve crush in (C) appears different from that in (B), likely reflecting some inter-study variability even within the same research team. SNC, sciatic nerve crush; DRC, dorsal root crush; SCI, spinal cord injury. ScRNA-Seq data source: Milich et al. 2021 (A); Tran et al., 2019 (B); Jacobi et al., 2022 (C); Avraham et al. 2021 (D). See also Figures S5–S7, which show the corresponding UMAP plots.

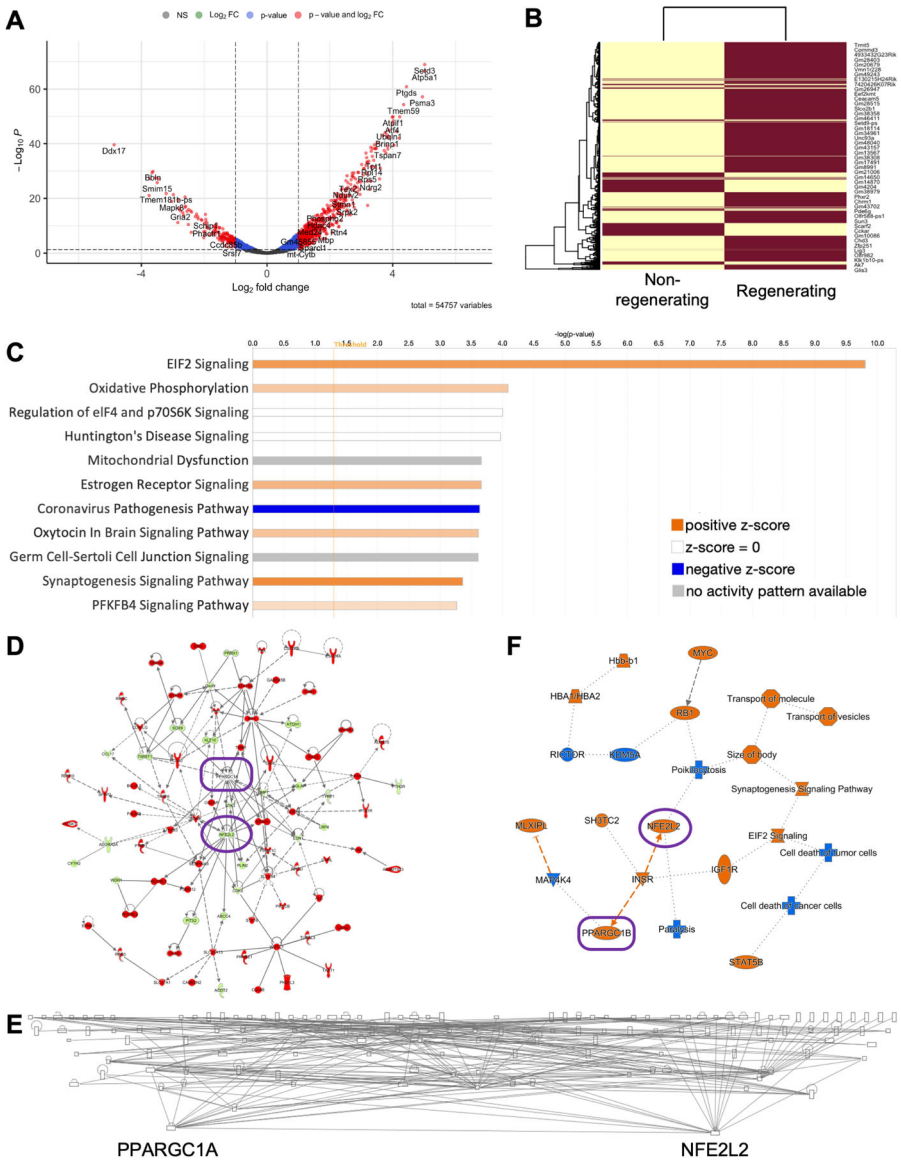

Figure 6. Bioinformatic analyses of differentially expressed genes identify *NFE2L2* and *PPARGC1A* as two central hubs in gene network.

(A) Volcano plot of differentially expressed (DE) genes. Large number of genes were significantly (adjusted p-value<0.05) overexpressed in regenerating neurons. (B) Heatmap of DE gene expression of regenerating and non-regenerating neurons (yellow: low; brown: high in regenerating neurons). (C) Top canonical pathways identified from DE genes between regenerating and non-regenerating CST neurons. EIF2 Signaling is the most significantly activated pathway followed by Oxidative Phosphorylation. (D) Gene network analysis with IPA using main genes with overexpressed and underexpressed genes indicates that NFE2L2 and PPARGC1A are represented as central regulators of these genes. Red: overexpressed genes; Green: underexpressed genes. Non-hub upstream genes are not shown. (E) Full network analysis illustrates NFE2L2 and PPARGC1A as two top regulators of DE genes. (F) Graphical summary of core analysis also implicates NFE2L2 as a hub in the network. Note that PPARGC1B (instead of PPARGC1A) is a node in this network.

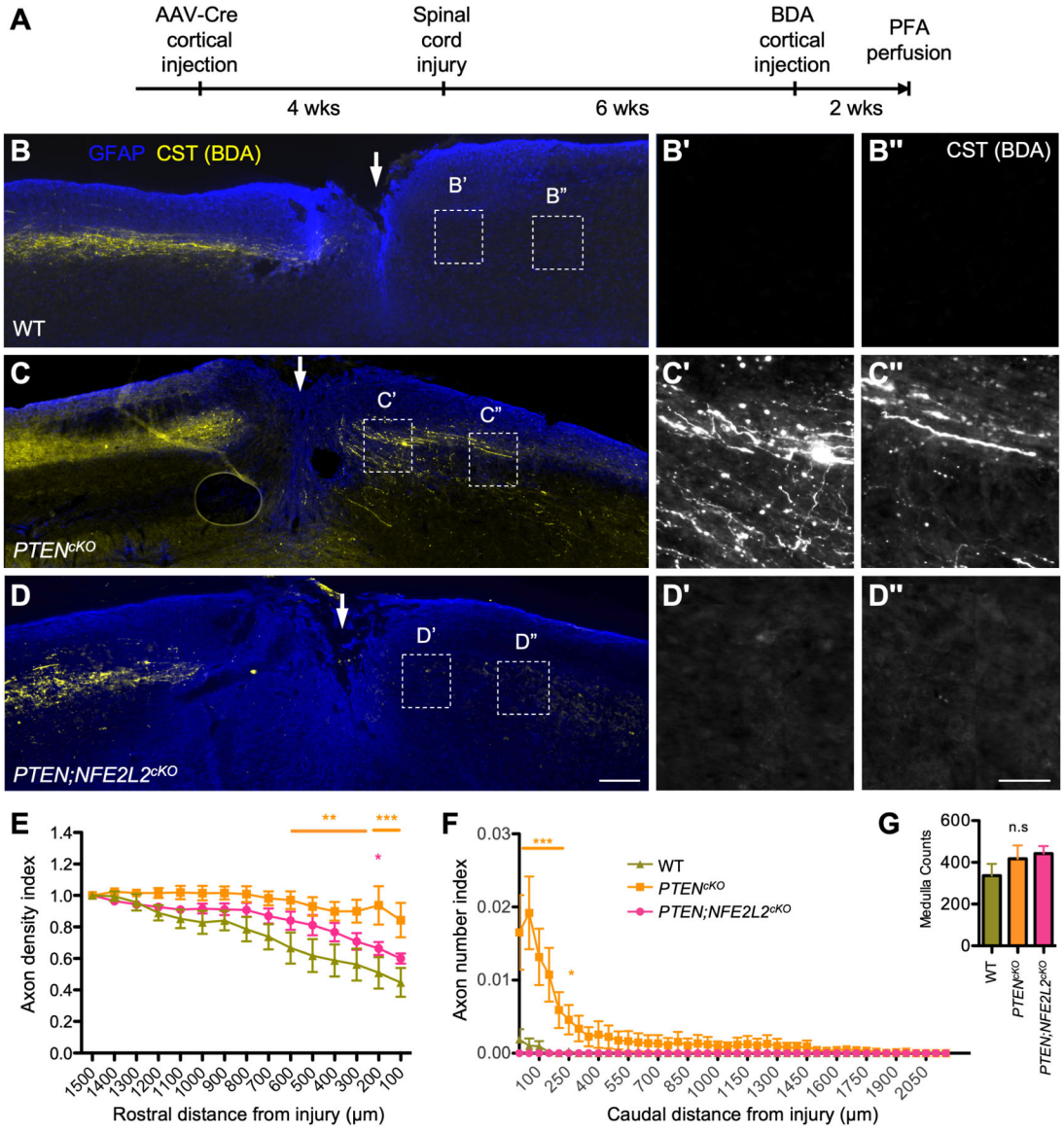

Figure 7. *NFE2L2* gene deletion substantially diminishes *PTEN* deletion-induced CST axon regeneration.

(A) Experimental timeline (B-D) Representative sagittal thoracic spinal cord sections showing BDA-traced CST axons at and around the T8 dorsal hemisection spinal cord injury site (arrow) from wild-type (WT), *PTEN* conditional knockout (cKO), and *PTEN;NFE2L2* double cKO mice. Rostral is to the left; caudal is to the right. Selected areas in dotted boxes in low magnification images on the left are shown at high magnification on the right. Scale bar = 300 μm (B-D, low mag), 100 μm (B'-D", high mag). (E) Quantification of axon density indices rostral to injury. Axon density indices were calculated as the average axon intensity at defined distances rostral to injury, and then normalized to axon density at 1.4–1.5 mm rostral to injury (mean ± SEM). Two-way RM ANOVA revealed significant differences across genetic conditions. Multiple comparisons with Bonferroni correction revealed elevated densities in *PTEN*^{cKO} multiple distance from injury site. **p < 0.01 at 600–300 μm; ***p < 0.001 at 200–100 μm. PTEN;NFE2L2^{cKO} showed significantly

elevated densities at 300 μm, *p < 0.05. (F) Quantification of axon number indices caudal to the injury site. Axon number indices were calculated as the average axon numbers at defined distances caudal to injury and then normalized to total axon count labeled in the medulla. Two-way RM ANOVA revealed statistically significant differences across genetic conditions. Multiple comparisons with Bonferroni correction revealed significantly elevated regeneration for *PTEN*^{cKO}: ***p < 0.001 at 50–200 μm, *p < 0.05 ; at 250 μm. Annotations for statistics for E and F: *p < 0.05, **p < 0.01, ***p < 0.001. (G) Quantification of total number of BDA labeled CST axons in medulla. N = 7 (WT), 10 (*PTEN*^{cKO}), 7 (*PTEN;NFE2L2*^{cKO}). See also Figures S9–S11.

KEY RESOURCES TABLE

REAGENT or RESOURCE	SOURCE	IDENTIFIER
Antibodies		
Rat anti mouse GFAP	Thermo Fisher Scientific	Cat# 130300; RRID: AB 2532994
Bacterial and virus strains		
AAV/retro-CAG-CRE-WPRE	Boston Children's Hospital	N/A
AAV/retro-CAG-GFP-WPRE	Boston Children's Hospital	N/A
AAV2.CAG-CRE-WPRE	Boston Children's Hospital	N/A
Biological Samples		
Normal Horse Serum	Vector Laboratories	Cat# S-2000
Triton X-100	Bio-Rad	Cat# 1610407
Cryo OCT	Fisher scientific	Cat# 1437365
Critical commercial assays		
Biotinylated Dextran, 10,000 MW,	Thermo Fisher Scientific	Cat# D1956
Superscript III	Thermo Fisher Scientific	Cat# 18080085
MEGAscript® T7 Transcription Kit	Thermo Fisher Scientific	Cat# AMB13345
RNasin (Promega) From VWR	VWR	Cat# PAN2515
Clean XP Beads	Beckman Coulter	Cat# A63987
TruSeq Stranded mRNA Sample Prep Kit	Illumina	Cat# RS-122–2101
AMPure Beads	Beckman Coulter	Cat# A63881
Superscript II	Thermo Fisher Scientific	Cat# 18064071
TSA Vivid™ Fluorophore Kit 520	Biotechne	Cat# 7523
TSA Vivid™ Fluorophore Kit 570	Biotechne	Cat# 7526
TSA™ Plus Fluorescein System	Perkin Elmer	Cat# NEL741001KT
VECTASTAIN® Elite® ABC-HRP Kit	Vector Laboratory	Cat# PK-6100
Deposited data		
Single cell sequencing data	This paper	GEO: GSE205769

REAGENT or RESOURCE	SOURCE	IDENTIFIER
Mendeley data for histology	This paper	https://data.mendeley.com/v1/datasets/10.17632/fvwzyvgnkb.1
Experimental models: Organisms/strains		
Mouse: PTENf, B6.129S4-Ptentm1Hwu/J	The Jackson Laboratory	Strain#: 006440
Mouse: SOCS3f, B6129S4-	The Jackson	Strain#: 010944
Socs3tm1Ayos/J	Laboratory	
Mouse: tdTomato, B6.Cg-Gt(ROSA)26Sortm14(CAG-tdTomato)Hze/J	The Jackson Laboratory	Strain#: 007914
Mouse:NFE2L2f, C57BL6-Nfe2l2tm1.1SredSbisJ	The Jackson Laboratory	Strain#: 025433
Oligonucleotides		
dT-T7 oligo: GGAGGCCGGAGAATTGTAATACGACTCACTATAGGGAGACGCGTGTTTTTTTTTTTTTTTTTTTTTTTTV	Li and Eberwine[84]	N/A
PTEN Forward: CAAGCACTCTGCGAACTGAG	The Jackson Laboratory	Strain#: 006440
PTEN Reverse: AAGTTTTTGAAGGCAAGATGC	The Jackson Laboratory	Strain#: 006440
SOCS3 Forward: CGGGCAGGGGAAGAGACTGT	The Jackson Laboratory	Strain#: 010944
SOCS3 Reverse: GGAGCCAGCGTGGATCTGC	Geoffroy et al.,[85]	N/A
ROSA26 Forward: AGGGAGCTGCAGTGGAGTA	The Jackson Laboratory	Strain#: 007914
ROSA26 Reverse: CCGAAAATCTGTGGGAAGTC	The Jackson Laboratory	Strain#: 007914
tdTomato Forward: CTGTTCCTGTACGGCATGG	The Jackson Laboratory	Strain#: 007914
WPRE Reverse: GGCATTAAAGCAGCGTATCC	The Jackson Laboratory	Strain#: 007914
NFE2L2 Forward: TCATGAGAGCTTCCCAGACTC	The Jackson Laboratory	Strain#: 025433
NFE2L2 Reverse: CAGCCAGCTGCTTGIIIIC	The Jackson Laboratory	Strain#: 025433
Recombinant DNA		
RNAscope® Probe - Mm-Nfe2l2 - musculus nuclear factor erythroid derived 2 like 2 (Nfe2l2) transcript variant 1 mRNA	Biotechne	Cat# 475571
RNAscope® Probe - Mm-Bcl11b-C3 - Mus musculus B cell leukemia/lymphoma 11B (Bcl11b) transcript variant 2 mRNA	Biotechne	Cat# 413271-C3
Random Primers (Promega) From VWR	VWR	Cat# PAC1181
Software and algorithms		
Codes for data processing including the application package for Regeneration Classifier	This paper	https://github.com/neurohugo/SingleCellPatchseqAnalysis
Zen Blue	Zeiss	N/A
R 3.6.2	R project	https://www.r-project.org/

REAGENT or RESOURCE	SOURCE	IDENTIFIER
STAR 2.7.10b	Dobin et al.,[86]	https://github.com/alexdobin/STAR
Samtools	Li H et al.,[87]	http://www.htslib.org/
htseq	Putri et al.,[88]	https://htseq.readthedocs.io/en/master/
DESeq2	Love et al.,[89]	https://bioconductor.org/packages/release/bioc/html/DESeq2.html
EdgeR	Robinson et al.,[90]	https://bioconductor.org/packages/release/bioc/html/edgeR.html
Ingenuity Pathway analysis	Qiagen	https://digitalinsights.qiagen.com/products-overview/discovery-insights-portfolio/analysis-and-visualization/qiagen-ipa/
Seurat 2.3.4 / 4.0	Butler et al.,[91]	https://satijalab.org/seurat/
Garnett	Pliner et al.,[25]	https://cole-trapnell-lab.github.io/garnett/
scRNAseq	Bioconductor	https://bioconductor.org/packages/release/data/experiment/html/scRNAseq.html
SingleR	Aran et al.,[23]	https://www.nature.com/articles/s41590-018-0276-y
Scater	McCarthy et al.,[92]	https://bioconductor.org/packages/release/bioc/html/scuttle.html
Panther Gene ontology	Ashburner et al.,[93]	http://geneontology.org/
ImageJ 2.9.0	Schneider et al.,[94]	https://github.com/imagej/imagej1
GraphPad Prism version 9.0	GraphPad software Inc.	https://www.graphpad.com/
Other		
Fluoromount-G	Southern Biotechnology	Cat# 0100–01
dNTP's (10 mM)	Thermo Fisher Scientific	Cat# R0193
5X Second strand buffer	Thermo Fisher Scientific	Cat# 10812014
DNA polymerase I	Thermo Fisher Scientific	Cat# 18010025
T4 DNA polymerase (5U/jl)	Thermo Fisher Scientific	Cat# 18005025
RNase H (2U/|jl)	Thermo Fisher Scientific	Cat# 18021071